

ON ℓ_1 DATA FITTING AND CONCAVE REGULARIZATION FOR IMAGE RECOVERY*

MILA NIKOLOVA[†], MICHAEL K. NG[‡], AND CHI-PAN TAM[§]

Abstract. We propose a new family of cost functions for signal and image recovery: they are composed of ℓ_1 data fitting terms combined with concave regularization. We exhibit when and how to employ such cost functions. Our theoretical results show that the minimizers of these cost functions are such that each one of their entries is involved either in an exact data fitting component or in a null component of the regularization part. This is a strong and particular property that can be useful for various image recovery problems. The minimization of such cost functions presents a computational challenge. We propose a fast minimization algorithm to solve this numerical problem. The experimental results show the effectiveness of the proposed algorithm. All illustrations and numerical experiments give a flavor of the possibilities offered by the minimizers of this new family of cost functions in solving specialized image processing tasks.

Key words. continuation methods, image recovery, inverse problems, ℓ_1 data fitting, MRI, multidimensional shrinkage, nonsmooth and nonconvex analysis, nonsmooth and nonconvex minimization, properties of minimizers, regularization, total variation, variable-splitting, penalty methods, variational methods

AMS subject classifications. 65F22, 65K05, 90C26, 90C53

DOI. 10.1137/10080172X

1. Introduction. Digital image restoration and reconstruction plays an important role in various fields such as medical and astronomical imaging, film restoration, image and video coding, and many others [22, 19]. We consider data production models where the observed data $v \in \mathbb{R}^q$ are related to the underlying $n \times m$ image, rearranged into a vector $u \in \mathbb{R}^p$ ($p = mn$), according to

$$(1) \quad v = Au \quad \text{with perturbations,}$$

where A is a $q \times p$ matrix which can, for instance, be the identity ($A = I$) or can model optical blurring, distortion wavelets in seismic imaging, X-ray tomography (an incomplete Radon transform), diffraction tomography (an underdetermined Fourier transform), and so on.

In most of these applications, the information provided by the forward model (1) alone is not sufficient to find an acceptable solution to this equation. Prior information on the underlying image is needed to find a convenient solution to (1)—that is, a solution which is close to (1) in an appropriate way and meets reasonable prior requirements. A flexible means of defining such a solution is regularization (see, e.g.,

*Submitted to the journal's Methods and Algorithms for Scientific Computing section July 12, 2010; accepted for publication (in revised form) August 22, 2012; published electronically January 24, 2013.

<http://www.siam.org/journals/sisc/35-1/80172.html>

[†]Centre de Mathématiques et de Leurs Applications (CMLA), ENS Cachan, CNRS, F-94230 Cachan Cedex, France (nikolova@cmla.ens-cachan.fr).

[‡]Corresponding author. Centre for Mathematical Imaging and Vision and Department of Mathematics, Hong Kong Baptist University, Kowloon Tong, Hong Kong (mng@math.hkbu.edu.hk). The research of this author was supported in part by a Hong Kong Research Grants Council grant and by Hong Kong Baptist University Faculty Research Grants.

[§]Centre for Mathematical Imaging and Vision and Department of Mathematics, Hong Kong Baptist University, Kowloon Tong, Hong Kong (cptam@math.hkbu.edu.hk).

[6, 18, 2]), where the sought-after solution, denoted in what follows by \hat{u} , is a minimizer of a cost function of the form

$$(2) \quad \Theta(u) + \beta\Phi(u),$$

where

$$(3) \quad \Phi(u) = \sum_{j=1}^r \varphi(\|G_j u\|_2).$$

In these expressions, Θ is called the *data fitting* term, and Φ the *regularization* (or penalty) term. In fact, Θ forces closeness to data v in accordance with (1), Φ embodies the priors, and $\beta > 0$ is a parameter that controls the trade-off between these two terms. In (3), for every $j \in \{1, \dots, r\}$, $G_j : \mathbb{R}^p \rightarrow \mathbb{R}^s$ is a linear operator where $s \geq 1$ is an integer. For instance, the family $\{G_j\} \equiv \{G_j\}_{j=1}^r$ can generate the discrete approximation of the gradient of an image u (then $s = 2$) or the Laplacian operator on u (in which case $s = 1$), or finite differences of various orders ($s = 1$), or the combination of any one of these with the synthesis operator of a frame transform. The function

$$\varphi : \mathbb{R}_+ \rightarrow \mathbb{R}$$

is *increasing*. It is usually called a potential function (PF). Quite varied functions φ have been used in the literature; a review can be found, for instance, in [8]. An important requirement is that φ allow the recovery of both relevant edges and smooth regions in the solution \hat{u} . For two decades, one of the most popular PFs has been $\varphi(t) = t$: when $\{G_j\}$ yields a discrete approximation of the gradient of u , Φ amounts to the discrete version of the *convex* nonsmooth *total variation* (TV) penalty [41]

$$(4) \quad \text{TV}(u) = \sum_{j=1}^r \|G_j u\|_2.$$

The most frequent choice for assessing fitting to data is the ℓ_2 -norm, $\Theta(\cdot) = \|\cdot\|_2^2$; see, e.g., the textbook [2]. We note that this quadratic data term Θ regularized with a TV-term unavoidably entails a bias with respect to the original image [42]. In 2002, some of the authors of this paper [32] showed that ℓ_1 data terms

$$(5) \quad \Theta(u) = \|Au - v\|_1$$

are useful in image processing *if some data equations in the linear system* (1) *have to be satisfied exactly*. Such a property is precious, for instance if data are corrupted with impulse noise [33, 4] or in hybrid restoration methods [12]. *Continuum* L_1 -TV energies $\|u - v\|_1 + \beta\text{TV}(u)$ for images of bounded variation, and more specifically when data v is the characteristic functions of a bounded domain, were studied by Chan and Esedoglu in [10]. They exhibited interesting contrast invariance properties of the minimizers of L_1 -TV: small features in the image remain intact up to some critical value of β , above which they suddenly disappear. Later on, L_1 -TV (or ℓ_1 -TV)-like energies were revealed to be successful in image decomposition [3, 14], for the recovery of binary images [11] or in segmentation, in optical flow image registration [38, 48, 45, 39], as well as in image restoration using hybrid methods [13]. Let us note that their minimizers were proven to be nonstrict in general [13]. Fast algorithms

devoted to the minimization of cost functions involving an ℓ_1 data fitting of the form (5) were developed; see, e.g., [15, 20, 13, 45].

Even though convex PFs give rise to *feasible* optimization problems [2], the numerical results in the pioneering work of Geman and Geman [18] have shown that nonconvex PFs φ offer richer possibilities for restoring high quality images. Since [16, 17], *concave* PFs, jointly with an ℓ_2 data fitting $\Theta(\cdot) = \|\cdot\|_2^2$, have been used in the literature; see, e.g., [31, 5, 25, 24, 35, 28, 9, 36], especially in connection with sparse recovery. A theoretical explanation of the interest of this form of cost functions was furnished in [34]. A general study on local convergence of descent methods for such nonconvex cost functions was recently provided in [1].

In this paper, we introduce a new class of cost functions: they combine an ℓ_1 data fitting, as given in (5), and a regularization term Φ of the form (3), defined using increasing and *strictly concave* PFs φ . Such cost functions are obviously nonconvex and nondifferentiable. Our goal is to explore the advantages of these cost functions. In this direction, this work provides two main contributions. The theoretical one is to prove that each entry $\hat{u}[k]$ of a (local) minimizer \hat{u} of such a cost function ensures that at least one data equation is fitted exactly, $a_i \hat{u} = v[i]$, where a_i is the i th row of A , or in (at least) one vanishing operator $G_j \hat{u} = 0$, or in both types of equations (see section 2). In the simple case when $A = I$ and $\{G_j\}$ are discrete gradients or first-order differences, minimizers are composed of (i) constant regions surrounded by closed contours and (ii) restored samples equal to the relevant data entries. The second main contribution of this article is to propose a fast algorithm for approximating the global minimizer of these cost functions (section 3). Our experimental results (section 4) clearly show the effectiveness and the efficiency of the proposed numerical scheme as well as the interest of this new family of cost functions. Concluding remarks are given in section 5.

2. Peculiar properties of minimizers. In this section, we study the main properties of the (local) minimizers \hat{u} of cost functions as defined by (2), (3), and (5). We denote by $a_i \in \mathbb{R}^{1 \times p}$ the i th row of A , for any $i \in \{1, \dots, q\}$. Then the i th component of Au is $(Au)[i] = a_i u$. Thus the cost functions $\mathcal{F} : \mathbb{R}^p \rightarrow \mathbb{R}$ in which we are interested read

$$(6) \quad \begin{aligned} v \in \mathbb{R}^q, \quad \mathcal{F}(u) &= \|Au - v\|_1 + \beta \Phi(u) \\ &= \sum_{i \in I} |a_i u - v[i]| + \beta \sum_{j \in J} \varphi(\|G_j u\|_2), \quad \beta > 0, \end{aligned}$$

$$\text{where} \quad \begin{aligned} I &\stackrel{\text{def}}{=} \{1, \dots, q\}, \\ J &\stackrel{\text{def}}{=} \{1, \dots, r\}. \end{aligned}$$

Without loss of generality, we assume that

$$a_i \neq 0 \quad \forall i \in I \quad \text{and} \quad G_j \neq 0 \quad \forall j \in J.$$

The matrix composed of all G_j , denoted by G , reads

$$(7) \quad G = [G_1^T, \dots, G_r^T]^T,$$

where the superscript “ T ” stands for the transpose. Usually $\text{rank } G < p$. For instance, if $\{G_j\}$ yields the discrete approximation of the gradient of u , then $\ker G = \text{span}(\mathbb{1})$,

where $\mathbb{1}$ is the vector composed of ones. We adopt the standard assumption enabling us to have regularization:

H1. $\ker A \cap \ker G = \{0\}$.

The function φ in (6) is *strictly increasing* and *concave* on $\mathbb{R}_+ \stackrel{\text{def}}{=} \{c \in \mathbb{R} \mid c \geq 0\}$. Hence $t \rightarrow \varphi(|t|)$ is nondifferentiable at zero. The precise assumptions on φ are listed below.

H2. *The function φ in (6) has the following properties:*

- (a) $\varphi : \mathbb{R}_+ \rightarrow \mathbb{R}_+$ is \mathcal{C}^2 on $\mathbb{R}_+^* \stackrel{\text{def}}{=} \mathbb{R}_+ \setminus \{0\}$ and $\varphi(t) > \varphi(0)$ for all $t > 0$;
- (b) $\varphi'(0^+) > 0$ and $\varphi'(t) > 0$ on \mathbb{R}_+^* ;
- (c) φ'' is increasing on \mathbb{R}_+^* , $\varphi''(t) < 0$ for all $t > 0$, and $\lim_{t \searrow 0} \varphi''(t) < 0$ is well defined and finite.

The condition that $\lim_{t \searrow 0} \varphi''(t) < 0$ be finite in H2(c) implies that $\varphi'(0^+) > 0$ in H2(b) is finite as well. Examples of functions φ satisfying H2 are given in Table 1 and plotted in Figure 1.

TABLE 1
Functions $\varphi : \mathbb{R}_+ \rightarrow \mathbb{R}_+$ satisfying H2.

	(f1)	(f2)	(f3)	(f4)
$\varphi(t)$	$\frac{\alpha t}{\alpha t + 1}$ $\alpha > 0$	$1 - \alpha^t$ $0 < \alpha < 1$	$\ln(\alpha t + 1)$ $\alpha > 0$	$(t + \varepsilon)^\alpha$ $0 < \alpha < 1, \varepsilon > 0$
$\varphi'(t)$	$\frac{\alpha}{(\alpha t + 1)^2}$	$-\alpha^t \ln \alpha > 0$	$\frac{\alpha}{\alpha t + 1}$	$\alpha(t + \varepsilon)^{\alpha-1}$
$\varphi'(0^+)$	α	$-\ln \alpha > 0$	α	$\alpha \varepsilon^{\alpha-1}$
$\varphi''(t)$	$\frac{-2\alpha^2}{(\alpha t + 1)^3}$	$-\alpha^t (\ln \alpha)^2$	$\frac{-\alpha^2}{(\alpha t + 1)^2}$	$\alpha(\alpha - 1)(t + \varepsilon)^{\alpha-2} < 0$
$\lim_{t \searrow 0} \varphi''(t)$	$-2\alpha^2$	$-(\ln \alpha)^2$	$-\alpha^2$	$\alpha(\alpha - 1)\varepsilon^{\alpha-2} < 0$

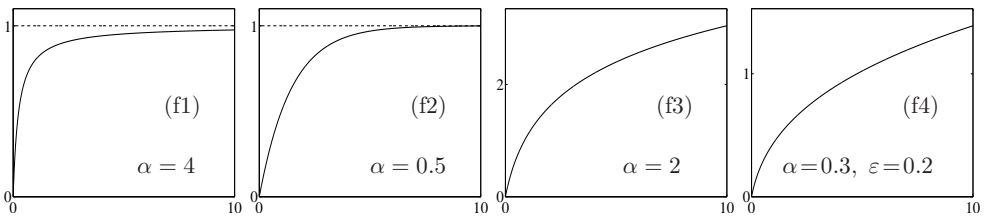


FIG. 1. *Plots of the PFs φ given in Table 1. Note that (f1) and (f2) are bounded above, which is not the case for (f3) and (f4).*

2.1. Motivation. Figures 2, 3, and 5 depict minimizers of \mathcal{F} in (2) for one-dimensional signals, where $A = I$, $\{G_j\}$ are first-order differences (hence H1 holds true) and different functions φ satisfying H2. These minimizers were obtained using a continuation algorithm like the one presented in section 3 where initialization was done with a null signal. In Figures 2, 3, and 5(b), \mathcal{F} is of the form (6), so it reads

$$(8) \quad \mathcal{F}(u) = \|u - v\|_1 + \beta \sum_{i=1}^{p-1} \varphi(|u[i+1] - u[i]|).$$

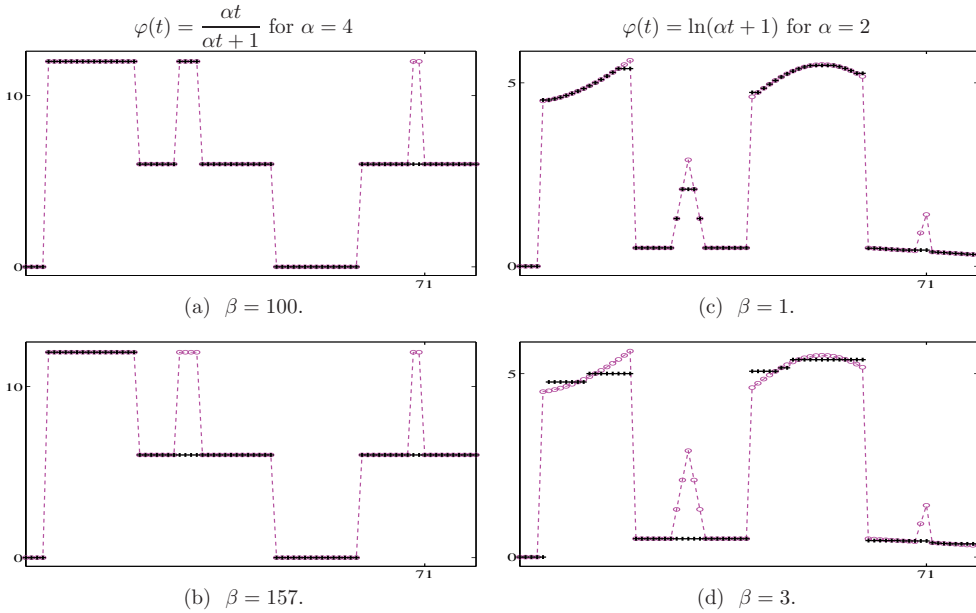


FIG. 2. Minimizers of \mathcal{F} in (8) for two functions φ obeying H2: (f1) for (a), (b) and (f3) for different values of β for (c), (d) as given. Data samples $v[i]$ are marked with (ooo), samples $\hat{u}[i]$ of the minimizer with (+++).

Figure 2 shows the minimizers for two different data vectors $v \in \mathbb{R}^{80}$ and functions φ and for different values of β . In the left column, φ is the function (f1) from Table 1. The numerical tests have shown that for any $\beta \in \{1, \dots, 78\}$ we have $\hat{u} = v$ and that the solution in (a) is obtained for any $\beta \in \{80, \dots, 156\}$. Similarly, the minimizer in (c) remains unchanged for any $\beta \in 0.1 \times \{10, \dots, 14\}$, whereas we have $\hat{u} = v$ for all $\beta \in 0.1 \times \{1, \dots, 3\}$. In both cases one observes that when β decreases, more data samples are fitted exactly, whereas when β increases, more piecewise constant structures are formed; i.e., fitting to the prior model is reinforced. In the left column, where data is piecewise constant, increasing β removes some small objects which for a smaller β were equal to the relevant data entries. This effect can be related to the contrast preservation of the widest *constant* objects in the data, studied theoretically for binary images in [10]. In the right column, increasing β introduces constant zones (i.e., where $G_j \hat{u} = 0$) in locally variable regions in the data v and removes small objects—e.g., both triangles are deleted in (d).

Figure 3 shows the results obtained by minimizing \mathcal{F} in (8) along with all functions φ given in Table 1. Since for all these functions φ the original signal (in green or marked with ---) matches the prior model in (8), we explore the possibility of recovering it from the data v (in magenta or marked with o o o), which contain Gaussian noise. We systematically selected the largest value of β enabling us to restore the tiny gate-shaped feature¹ ending at sample 71. All minimizers (marked in black +++) in the figure are piecewise constant. The zooms in Figure 4 show that each constant piece fits *at most* one data entry. In particular, (a) and (b) in the first row do not fit any data sample, and the restored level is quite precise; in (a) it

¹Recall the experiment in Figure 2(a) and (b). In the present experiment, the tiny gate disappears for a slightly larger value of β .

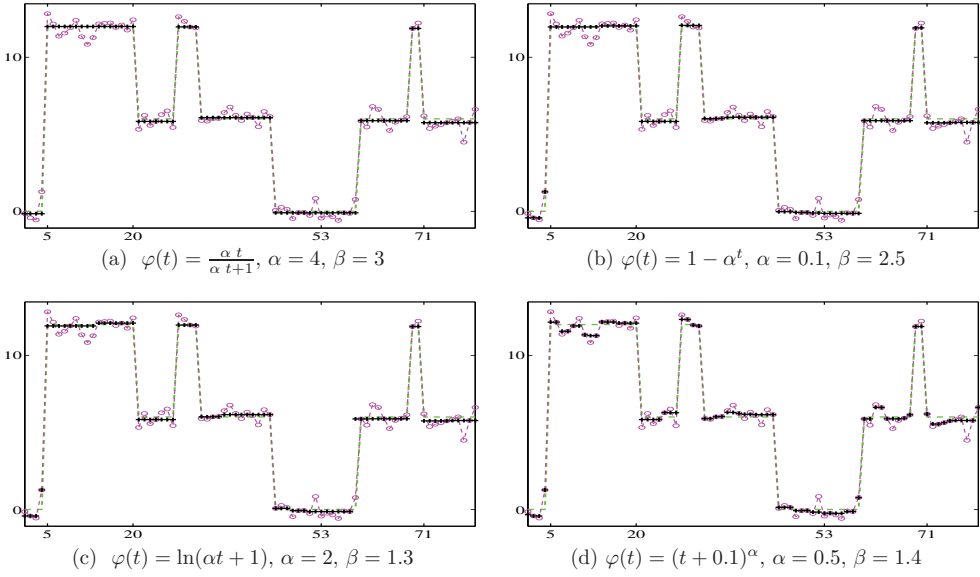


FIG. 3. Minimizers of \mathcal{F} as given in (8) for all functions φ evoked in Table 1. Data are corrupted with Gaussian noise. Data samples $v[i]$ are marked with $(\circ\circ)$, samples $\hat{u}[i]$ of the minimizer with $(+++)$. The original signal is also recalled $(- - -)$.

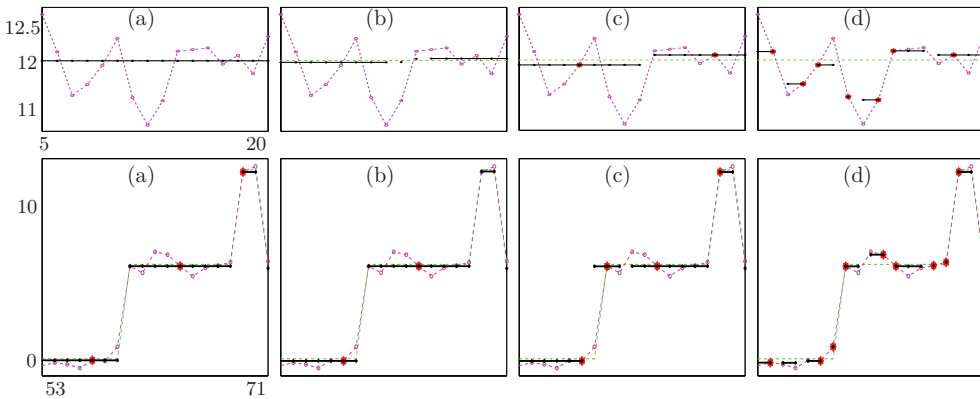


FIG. 4. Zooms of the plots in Figure 3. First row: samples 5–20. Second row: samples 53–71. Constant pieces are indicated using a solid black line. Data points $v[i]$ fitted exactly by the corresponding minimizers \hat{u} are shown using (\blacklozenge) . Data samples $v[i]$ are marked with $(\circ\circ)$, and samples $\hat{u}[i]$ of the minimizer with $(+++)$. The original signal is also recalled $(- - -)$.

seems to overlap the original one. These plots correspond to (f1) and (f2) in Table 1, which are bounded above. Comparing all results in Figure 3 (as well as the zooms in Figure 4), it appears that a faster increase of φ on \mathbb{R}_+ entails a degradation of the restoration quality. Among all tested functions, (f4) has the fastest increase on \mathbb{R}_+ , and the corresponding minimizer in (d) provides the worst restoration. The bounded above functions (f1) and (f2) seem to give rise to the best results.

In Figure 5 we compare ℓ_1 data fitting to quadratic ℓ_2 (smooth) fitting, using the same function (f1) in Table 1. In accordance with the results proven in [32, 33], one observes that even though the prior term is appropriate in both cases, quadratic

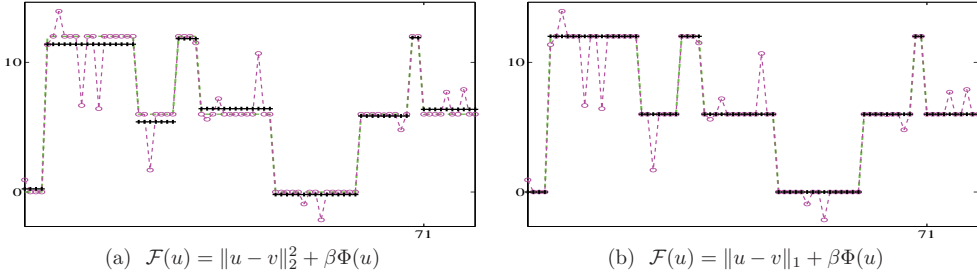


FIG. 5. In both cases, $\Phi(u) = \sum_{i=1}^{p-1} \varphi(|u[i+1] - u[i]|)$ where $\varphi(t) = \frac{\alpha t}{\alpha t + 1}$ for $\alpha = 4$. Data contain 20% impulse noise. Data samples $v[i]$ are marked with $(\circ\circ)$, samples $\hat{u}[i]$ of the minimizer with $(++)$. The original signal is reminded in $(- - -)$.

ℓ_2 data fitting does not enable a correct restoration of the original signal. A fully satisfying recovery is provided by the cost function that we propose.

Figures 3 and 5 show that (f1) in Table 1 gives rise to the best results in all tests. This is an important argument for using (f1) in the experiments in section 4.

Example 1 (scalar case). This example furnishes a first intuition on the reasons underlying the phenomena observed in Figures 2, 3, and 5. Given $v \in \mathbb{R}$, consider the following function $\mathcal{F} : \mathbb{R} \rightarrow \mathbb{R}$:

$$(9) \quad \mathcal{F}(u) = |u - v| + \beta\varphi(|u|) \quad \text{for } \varphi \text{ meeting H2.}$$

The necessary conditions for \mathcal{F} to have a (local) minimum at $\hat{u} \neq 0$ and $\hat{u} \neq v$ —that its first differential meets $D\mathcal{F}(\hat{u}) = 0$ and that its second differential obeys $D^2\mathcal{F}(\hat{u}) \geq 0$ —do not hold:

$$\hat{u} \notin \{0, v\} \quad \Rightarrow \quad \begin{cases} D\mathcal{F}(\hat{u}) = \text{sign}(\hat{u} - v) + \beta\varphi'(|\hat{u}|)\text{sign}(\hat{u}) = 0, \\ D^2\mathcal{F}(\hat{u}) = \beta\varphi''(|\hat{u}|) < 0, \end{cases}$$

where the last inequality comes from the concavity of φ on \mathbb{R}_+^* ; see H2(c). Hence, \mathcal{F} cannot have a minimizer such that $\hat{u} \neq 0$ and $\hat{u} \neq v$ for any $v \in \mathbb{R}$. Being coercive, \mathcal{F} does have minimizers. Consequently, any minimizer of \mathcal{F} in (9) satisfies

$$(10) \quad \hat{u} \in \{0, v\}.$$

For $\varphi(u) = \frac{\alpha u}{1 + \alpha u}$, the local and the global minimizers of \mathcal{F} in (9) can be calculated explicitly.²

The practical interest of cost functions of the form (6) can be appreciated thanks to the experiments provided in section 4.

²Let φ in (9) read $\varphi(u) = \frac{\alpha u}{1 + \alpha u}$. Using (10), the two possible (local) minimizers are $\hat{u}_1 = 0 \Rightarrow \mathcal{F}(\hat{u}_1) = |v|$ and $\hat{u}_2 = v \Rightarrow \mathcal{F}(\hat{u}_2) = \beta\varphi(|v|) = \mathcal{F}(\hat{u}_2) = \beta \frac{\alpha|v|}{1 + \alpha|v|}$. In consequence, the global minimizer \hat{u} of \mathcal{F} fulfills one of the following three options: (i) $\hat{u} = \hat{u}_1 = 0 \Leftrightarrow \mathcal{F}(\hat{u}_1) < \mathcal{F}(\hat{u}_2) \Leftrightarrow |v| < \beta \frac{\alpha|v|}{1 + \alpha|v|} \Leftrightarrow |v| < \beta - \frac{1}{\alpha}$, (ii) $\hat{u} = \{0, v\} \Leftrightarrow \mathcal{F}(\hat{u}_1) = \mathcal{F}(\hat{u}_2) \Leftrightarrow |v| = \beta - \frac{1}{\alpha}$, or (iii) $\hat{u} = \hat{u}_2 = v \Leftrightarrow \mathcal{F}(\hat{u}_1) > \mathcal{F}(\hat{u}_2) \Leftrightarrow |v| > \beta - \frac{1}{\alpha}$. The cost function \mathcal{F} has two distinct global minimizers only for two values of v , namely $v = \beta - \frac{1}{\alpha}$ and $v = -\beta + \frac{1}{\alpha}$. The set of these points is closed, and its Lebesgue measure in the space of v , namely \mathbb{R}^1 , is null. Observe also that if $\beta\alpha < 1$, we have $\hat{u} = v$ for any real v .

2.2. Preliminary results. We first verify that cost functions \mathcal{F} of the form (6) do have minimizers.

PROPOSITION 1. *Let \mathcal{F} read as in (6). Assume that H1 holds and that φ satisfies H2. Then for any v the optimal set $\hat{U} \stackrel{\text{def}}{=} \{\hat{u} \in \mathbb{R}^p \mid \mathcal{F}(\hat{u}) = \inf_{u \in \mathbb{R}^p} \mathcal{F}(u)\}$ is nonempty.*

The proof of this proposition is outlined in Appendix 6.1. Below it is illustrated using a 3-pixels example.

Example 2. Let \mathcal{F} be of the form (6) for $p = 3$ and $q = 2$, where

$$(11) \quad A = \begin{bmatrix} 1 & 0 & 0 \\ 0 & 0 & 1 \end{bmatrix}, \quad v = \begin{bmatrix} 1 \\ 3 \end{bmatrix}, \quad G_1 = \begin{bmatrix} 1 & -1 & 0 \\ 0 & 1 & -1 \end{bmatrix}, \quad \varphi(t) = \frac{\alpha|t|}{\alpha|t| + \alpha}.$$

Thus \mathcal{F} reads

$$\mathcal{F}(u) = |u[1] - v[1]| + |u[3] - v[2]| + \beta(\varphi(|u[1] - u[2]|) + \varphi(|u[2] - u[3]|)).$$

Note that $\text{rank } A = \text{rank } G = 2 < p = 3$ and that φ , obeying H2, is bounded above. We have

$$\ker A = \{w \in \mathbb{R}^3 \mid w = [0 \ c \ 0], \ c \in \mathbb{R}\} \quad \text{and} \quad \ker G = c\mathbb{1} \in \mathbb{R}^3, \ c \in \mathbb{R},$$

and hence H1 is satisfied since $\ker A \cap \ker G = \{0\}$. One computes (by hand) that for $\alpha = 1$ and $\beta = 2$ the global minimizer of \mathcal{F} reads

$$(12) \quad \hat{u} = [1 \ 1 \ 3]^T.$$

Given $v \in \mathbb{R}^q$, with each $\hat{u} \in \mathbb{R}^p$ we systematically associate the following subsets:

$$(13) \quad \begin{aligned} \hat{I}_0 &\stackrel{\text{def}}{=} \{i \in I \mid a_i \hat{u} = v[i]\} & \text{and} & \quad \hat{I}_0^c &\stackrel{\text{def}}{=} I \setminus \hat{I}_0 = \{i \in I \mid a_i \hat{u} \neq v[i]\}, \\ \hat{J}_0 &\stackrel{\text{def}}{=} \{i \in J \mid G_i \hat{u} = 0\} & \text{and} & \quad \hat{J}_0^c &\stackrel{\text{def}}{=} J \setminus \hat{J}_0 = \{i \in J \mid G_i \hat{u} \neq 0\}. \end{aligned}$$

Note that $G_i \hat{u} = 0 \in \mathbb{R}^s$ is equivalent to $\|G_i \hat{u}\|_2 = 0$; for $s = 1$ it is the same as $|G_i \hat{u}| = 0$.

Example 3. Let us consider Example 2 yet again. Clearly $I = \{1, 2\}$ and $J = \{1, 2\}$. For the global minimizer \hat{u} in (12) one finds that

$$(14) \quad \begin{aligned} \hat{I}_0 &= \{1, 2\} = I & \text{and} & \quad \hat{I}_0^c &= \emptyset, \\ \hat{J}_0 &= \{1\} & \text{and} & \quad \hat{J}_0^c &= \{2\}. \end{aligned}$$

Remark 1. If $v = 0$, it is clear that \mathcal{F} in (6) is minimized by $\hat{u} = v = 0$ since $\mathcal{F}(\hat{u}) = r\beta\varphi(0)$ is the least possible value of \mathcal{F} . For this trivial solution, $\hat{I}_0 = I$ and $\hat{J}_0 = J$, so $\hat{I}_0^c = \hat{J}_0^c = \emptyset$.

In what follows, we consider that $v \neq 0$, without further reminder.

For $(u, v) \in \mathbb{R}^p \times \mathbb{R}^q$, define

$$(15) \quad \psi_i(u) \stackrel{\text{def}}{=} |a_i u - v[i]|, \quad i \in I,$$

$$(16) \quad \phi_i(u) \stackrel{\text{def}}{=} \varphi(\|G_i u\|_2), \quad i \in J.$$

LEMMA 1. Let \mathcal{F} read as in (6). For a $\hat{u} \in \mathbb{R}^p$ we adopt the notation in (13) and assume that $\hat{I}_0^c \cup \hat{J}_0^c \neq \emptyset$. Put

$$\rho \stackrel{\text{def}}{=} \begin{cases} \min \left\{ \min_{i \in \hat{I}_0^c} \frac{|a_i \hat{u} - v[i]|}{\|a_i\|_2}, \min_{j \in \hat{J}_0^c} \frac{\|G_j \hat{u}\|_2}{\|G_j\|_2} \right\} & \text{if } \hat{I}_0^c \neq \emptyset \text{ and } \hat{J}_0^c \neq \emptyset; \\ \min \left\{ 1, \min_{j \in \hat{J}_0^c} \frac{\|G_j \hat{u}\|_2}{\|G_j\|_2} \right\} & \text{if } \hat{I}_0^c = \emptyset \text{ and } \hat{J}_0^c \neq \emptyset; \\ \min \left\{ \min_{i \in \hat{I}_0^c} \frac{|a_i \hat{u} - v[i]|}{\|a_i\|_2}, 1 \right\} & \text{if } \hat{I}_0^c \neq \emptyset \text{ and } \hat{J}_0^c = \emptyset. \end{cases}$$

Clearly $\rho > 0$. Let $u \in B(\hat{u}, \rho) \stackrel{\text{def}}{=} \{w \in \mathbb{R}^p \mid \|w - \hat{u}\|_2 < \rho\}$. Then

(17) $i \in \hat{I}_0^c \neq \emptyset \Rightarrow \psi_i(u) \in \mathcal{C}^2(B(\hat{u}, \rho));$

(18) $j \in \hat{J}_0^c \neq \emptyset \Rightarrow \phi_j(u) \in \mathcal{C}^2(B(\hat{u}, \rho)).$

In words, ψ_i for all $i \in \hat{I}_0^c$ and ϕ_j for all $j \in \hat{J}_0^c$, as given in (15) and (16), respectively, are \mathcal{C}^2 -smooth on the open ball $B(\hat{u}, \rho)$. This easy lemma is proven in Appendix 6.2.

The next remark furnishes some standard calculations that are needed for later use.

Remark 2. Let \mathcal{F} be of the form (6) and let assumption H2 hold. For a $\hat{u} \in \mathbb{R}^p$ consider the notation in (13). Then for any $w \in \mathbb{R}^p$ we have³

$$\begin{aligned} \text{(a)} \quad i \in \hat{I}_0^c &\implies \begin{cases} D\psi_i(\hat{u})w &= \text{sign}(a_i \hat{u} - v[i]) a_i w, \\ \langle D^2\psi_i(\hat{u})w, w \rangle &= 0, \end{cases} \\ \text{(b)} \quad j \in \hat{J}_0^c &\implies \begin{cases} D\phi_j(\hat{u})w &= \varphi'(\|G_j \hat{u}\|_2) \frac{\langle G_j \hat{u}, G_j w \rangle}{\|G_j \hat{u}\|_2}, \\ \langle D^2\phi_j(\hat{u})w, w \rangle &= \varphi''(\|G_j \hat{u}\|_2) \left(\frac{\langle G_j \hat{u}, G_j w \rangle}{\|G_j \hat{u}\|_2} \right)^2 \\ &\quad + \varphi'(\|G_j \hat{u}\|_2) \frac{\|G_j w\|_2^2 \|G_j \hat{u}\|_2^2 - \langle G_j \hat{u}, G_j w \rangle^2}{\|G_j \hat{u}\|_2^3}; \end{cases} \\ \text{(b')} \quad j \in \hat{J}_0^c \text{ and } G_j \in \mathbb{R}^{1 \times p} &\stackrel{\text{by (b)}}{\implies} \begin{cases} D\phi_j(\hat{u})w &= \varphi'(|G_j \hat{u}|) |G_j w|, \\ \langle D^2\phi_j(\hat{u})w, w \rangle &= \varphi''(|G_j \hat{u}|) (G_j w)^2. \end{cases} \end{aligned}$$

The next proposition justifies the notation introduced in (13) when analyzing the cost functions proposed in this work.

PROPOSITION 2. For \mathcal{F} as in (6) satisfying H2, let \hat{u} be a (local) minimizer of \mathcal{F} . Then

$$(\hat{I}_0 \cup \hat{J}_0) \neq \emptyset.$$

Proof. Suppose, on the contrary, that

(19) $\hat{I}_0 = \emptyset \text{ and } \hat{J}_0 = \emptyset.$

³Note that if $i \in \hat{I}_0^c$, then $\langle D^2\psi_i(\hat{u})w, w \rangle = \lim_{t \rightarrow 0} \frac{\text{sign}(a_i(\hat{u} + tw) - v[i]) a_i w - \text{sign}(a_i \hat{u} - v[i]) a_i w}{t} = 0.$

By Lemma 1, \mathcal{F} is \mathcal{C}^2 on a neighborhood of \hat{u} since $\hat{I}_0^c = I$ and $\hat{J}_0^c = J$. Using Remark 2, for $w = \hat{u}$ one finds that⁴

$$\begin{aligned} \langle D^2\mathcal{F}(\hat{u}, v)\hat{u}, \hat{u} \rangle &= \sum_{i \in I} \langle D^2\psi_i(\hat{u})\hat{u}, \hat{u} \rangle + \sum_{j \in J} \langle D^2\phi_j(\hat{u})\hat{u}, \hat{u} \rangle \\ &= \sum_{j \in J} \left(\varphi''(\|G_j\hat{u}\|_2) \left(\frac{\langle G_j\hat{u}, G_j\hat{u} \rangle}{\|G_j\hat{u}\|_2} \right)^2 \right. \\ &\quad \left. + \varphi'(\|G_j\hat{u}\|_2) \frac{\|G_j\hat{u}\|_2^2 \|G_j\hat{u}\|_2^2 - \langle G_j\hat{u}, G_j\hat{u} \rangle^2}{\|G_j\hat{u}\|_2^3} \right) \\ &= \sum_{j \in J} \varphi''(\|G_j\hat{u}\|_2) \left(\frac{\langle G_j\hat{u}, G_j\hat{u} \rangle}{\|G_j\hat{u}\|_2} \right)^2 < 0, \end{aligned}$$

where the last inequality is due to assumption H2(c). It shows that \hat{u} is not a (local) minimizer of \mathcal{F} (see, e.g., [40]). Consequently, the assumption in (19) is false. Hence the statement of the proposition. \square

When $\text{rank } G < p$ —an usual case—a user would not like to get (local) minimizers \hat{u} of \mathcal{F} that belong to $\ker G$ since these are meaningless solutions. A sufficient condition for avoiding such situations is given in the lemma stated next.

LEMMA 2. *Let \mathcal{F} in (6) meet H2 and $\text{rank } G < p$. Assume that data $v \in \mathbb{R}^q$ satisfy*

$$(20) \quad w \in \ker G \setminus \{0\} \Rightarrow a_i w \neq v[i] \quad \forall i \in I.$$

Let $\hat{u} \neq 0$ be such that $\hat{I}_0 \neq \emptyset$. Then

$$(21) \quad \hat{J}_0^c \neq \emptyset.$$

Proof. Suppose on the contrary that

$$(22) \quad \hat{J}_0 = J.$$

Then $\hat{u} \in \ker G \setminus \{0\}$, and (20) leads to $\hat{I}_0 = \emptyset$. Hence a contradiction with the assumption that $\hat{I}_0 \neq \emptyset$. This entails (21), where the equivalence relation comes from (13). \square

It is worth emphasizing that the assumption in (20) is typically satisfied.⁵ For instance, consider that G corresponds to first-order differences or a discrete gradient. Then $\ker G = \text{span}(\mathbb{1})$ and (20) means that $v \neq cA\mathbb{1}$ for any real c .

If $\ker G = \{0\}$, it is clear that (21) is satisfied if $\hat{u} \neq 0$.

2.3. Discarding perilous nonminimizer points. Given $v \in \mathbb{R}^q$, with any $\hat{u} \in \mathbb{R}^p$, we *systematically* associate the following *linear* manifolds by using the notation in (13):

$$(23) \quad \mathcal{K}_{\hat{u}} = \{w \in \mathbb{R}^p \mid a_i w = v[i] \ \forall i \in \hat{I}_0 \text{ and } G_i w = 0 \ \forall i \in \hat{J}_0\},$$

$$(24) \quad \mathcal{K}_{\hat{u}} = \{w \in \mathbb{R}^p \mid a_i w = 0 \ \forall i \in \hat{I}_0 \text{ and } G_i w = 0 \ \forall i \in \hat{J}_0\}.$$

⁴If $s = 1$, i.e., $G_j \in \mathbb{R}^{1 \times p}$ for all $j \in J$, Remark 2(a)–(b') and H2(c) show that for any $w \in \mathbb{R}^p$ $\langle D^2\mathcal{F}(\hat{u}, v)w, w \rangle = \sum_{j \in J} \varphi''(\|G_j\hat{u}\|) (G_j w)^2 < 0$.

⁵A little effort is needed to show that data v that fail (20) belong to a closed subset of Lebesgue measure zero in \mathbb{R}^q , since the dimension of $\ker G$ is typically very small compared to $\min\{p, q\}$.

Since

$$\hat{u} \in \mathcal{K}_{\hat{u}},$$

we have $\mathcal{K}_{\hat{u}} \neq \emptyset$. Note that $K_{\hat{u}}$ is the vector subspace tangent to $\mathcal{K}_{\hat{u}}$; hence

$$(25) \quad \hat{u} + w \in \mathcal{K}_{\hat{u}} \quad \forall w \in K_{\hat{u}}.$$

Remark 3. Proposition 2 tells us that any (local) minimizer \hat{u} of \mathcal{F} belongs to a nonempty manifold $\mathcal{K}_{\hat{u}}$ of the form (23).

Nevertheless, there may be other points $\hat{u} \in \mathbb{R}^p$ that also give rise to a nonempty $\mathcal{K}_{\hat{u}}$ but which are *not* (local) minimizers of \mathcal{F} . In this subsection, we describe the latter kind of (dangerous) points. To this end, we examine the restriction of \mathcal{F} to the manifold $\mathcal{K}_{\hat{u}}$, say $F \stackrel{\text{def}}{=} \mathcal{F}|_{\mathcal{K}_{\hat{u}}}$,

$$(26) \quad \begin{aligned} F : \mathcal{K}_{\hat{u}} &\rightarrow \mathbb{R}, \\ F(u) &= \sum_{i \in \hat{I}_0^c} |a_i u - v[i]| + \beta \sum_{j \in \hat{J}_0^c} \varphi(\|G_j u\|_2). \end{aligned}$$

According to Lemma 1, F is \mathcal{C}^2 on a neighborhood of \hat{u} .

Using the notation in (13), we also suppose that the following holds.

H3. *The point $\hat{u} \in \mathbb{R}^p$ is such that $\hat{I}_0 \neq \emptyset$ and that⁶*

$$(27) \quad w \in \ker G \setminus \{0\} \Rightarrow \exists i \in \hat{I}_0 \text{ such that } a_i w \neq 0.$$

The assumption in (27) might seem tricky. However, it can be seen as a restriction of a more general assumption, namely,

$$(28) \quad w \in \ker G \setminus \{0\} \Rightarrow a_i w \neq 0 \quad \forall i \in I.$$

The latter holds true in most of the applications. A relevant example is when A and G are the discrete versions of an integral and a differential operator, respectively. For example, if $\ker G = \text{span}(\mathbb{1})$, (28) means that $a_i \mathbb{1} \neq 0$ for all $i \in I$.

LEMMA 3. *For $\hat{u} \in \mathbb{R}^p$, we posit the definitions of \hat{I}_0 and \hat{J}_0^c (see (13)), as well as the one of $K_{\hat{u}}$ in (24). Let H3 hold and $\hat{J}_0^c \neq \emptyset$. Suppose that the dimension of $K_{\hat{u}}$ satisfies $\dim K_{\hat{u}} \geq 1$. Then*

$$w \in K_{\hat{u}} \setminus \{0\} \Rightarrow \hat{J}_0^c(w) \stackrel{\text{def}}{=} \{j \in \hat{J}_0^c \mid G_j w \neq 0\} \neq \emptyset.$$

Proof. If $\ker G = \{0\}$, the result is obvious. Let $\text{rank } G < p$. The proof is conducted by contradiction. So suppose that

$$(29) \quad \exists w \in K_{\hat{u}} \setminus \{0\} \text{ such that } G_j w = 0 \quad \forall j \in \hat{J}_0^c.$$

Combining (29) and the definition of $K_{\hat{u}}$ shows that $G_j w = 0$ for all $j \in \hat{J}_0^c \cup \hat{J}_0$; that is,

$$w \in \ker G \setminus \{0\}.$$

Using H3, there exists $i \in \hat{I}_0$ obeying $a_i w \neq 0$. But the definition of $K_{\hat{u}}$ shows that $w \notin K_{\hat{u}}$. It follows that (29) is false. Hence the result. \square

⁶Note that if $\text{rank } G = p$, the implication in (27) is trivial.

The cases when all operators G_j are one-dimensional row vectors and when $\{G_j\}$ contains some matrices $G_j \in \mathbb{R}^{s \times p}$ for $s \geq 2$ are considered separately. The former case is much easier to study.

LEMMA 4. Consider \mathcal{F} in (6), where $G_j \in \mathbb{R}^{1 \times p}$ for all $j \in J$ (i.e., $s = 1$) and H2 holds. Let $\hat{u} \in \mathbb{R}^p$ satisfy H3 and $\hat{J}_0^c \neq \emptyset$. Suppose that $\dim K_{\hat{u}} \geq 1$, where $K_{\hat{u}}$ is defined according to (24). Then the restricted function $F \stackrel{\text{def}}{=} \mathcal{F}|_{K_{\hat{u}}}$ (see (26)) satisfies

$$\langle D^2F(\hat{u})w, w \rangle < 0 \quad \forall w \in K_{\hat{u}} \setminus \{0\}.$$

Proof. Using Remark 2(a)–(b’), Lemma 3, and H2(c), it is straightforward that

$$w \in K_{\hat{u}} \setminus \{0\} \Rightarrow \langle D^2F(\hat{u})w, w \rangle = \beta \sum_{j \in \hat{J}_0^c(w)} \varphi''(|G_j \hat{u}|) (G_j w)^2 < 0.$$

The proof is complete. \square

The connection with Example 1 is obvious from the fact that F is the smooth part of \mathcal{F} .

Remark 4. When $G_j \hat{u} \neq 0$ and $G_j w \neq 0$ for $w \in K_{\hat{u}} \setminus \{0\}$, we have

$$\frac{\|G_j w\|_2^2 \|G_j \hat{u}\|_2^2}{\langle G_j \hat{u}, G_j w \rangle^2} > 1.$$

Indeed, $\hat{u} \in K_{\hat{u}}$ and $w \in K_{\hat{u}} \setminus \{0\}$, so $K_{\hat{u}} \neq K_{\hat{u}}$, in which case Schwarz’s inequality yields $|\langle G_j \hat{u}, G_j w \rangle| < \|G_j w\|_2 \|G_j \hat{u}\|_2$.

This remark is behind the additional assumptions (a)–(b) in the next lemma.

LEMMA 5. Let \mathcal{F} be of the form (6), where $\{G_j\}$ contains some matrices $G_j \in \mathbb{R}^{s \times p}$ for $s \geq 2$, and let H2 hold. Suppose that \hat{u} meets $\hat{J}_0^c \neq \emptyset$ and H3. We denote

$$\tau_0 \stackrel{\text{def}}{=} \min_{j \in \hat{J}_0^c} \|G_j \hat{u}\|_2 > 0 \quad \text{and} \quad \tau_1 \stackrel{\text{def}}{=} \max_{j \in \hat{J}_0^c} \|G_j \hat{u}\|_2 > 0.$$

Consider that (a) and (b) stated below are verified:

(a) There is a constant $C > 1$ such that

$$w \in K_{\hat{u}} \setminus \{0\} \Rightarrow \frac{\|G_j w\|_2^2 \|G_j \hat{u}\|_2^2}{\langle G_j \hat{u}, G_j w \rangle^2} \leq C \quad \forall j \in \hat{J}_0^c(w),$$

where $\hat{J}_0^c(w)$ is described in Lemma 3.

(b) The function φ is such that

$$\varphi''(t) + (C - 1) \frac{\varphi'(t)}{t} < 0, \quad \text{either } \forall t \geq \tau_0 \text{ or } \forall t \leq \tau_1.$$

Assume that $\dim K_{\hat{u}} \geq 1$ for $K_{\hat{u}}$, as given in (24). Then $F \stackrel{\text{def}}{=} \mathcal{F}|_{K_{\hat{u}}}$ (see (26)) satisfies

$$\langle D^2F(\hat{u})w, w \rangle < 0 \quad \forall w \in K_{\hat{u}} \setminus \{0\}.$$

Proof. Using Remark 2 and Lemma 3, as well as H2(c), the following chain of

inequalities is derived:

$$\begin{aligned}
 & \langle D^2F(\hat{u})w, w \rangle \\
 &= \beta \sum_{j \in \widehat{\mathcal{J}}_0^c} \varphi''(\|G_j \hat{u}\|_2) \left(\frac{\langle G_j \hat{u}, G_j w \rangle}{\|G_j \hat{u}\|_2} \right)^2 \\
 &+ \beta \sum_{j \in \widehat{\mathcal{J}}_0^c} \varphi'(\|G_j \hat{u}\|_2) \frac{\|G_j w\|_2^2 \|G_j \hat{u}\|_2^2 - \langle G_j \hat{u}, G_j w \rangle^2}{\|G_j \hat{u}\|_2^3} \\
 (\text{Lemma 3}) &= \beta \sum_{j \in \widehat{\mathcal{J}}_0^c(w)} \varphi''(\|G_j \hat{u}\|_2) \left(\frac{\langle G_j \hat{u}, G_j w \rangle}{\|G_j \hat{u}\|_2} \right)^2 \\
 &+ \beta \sum_{j \in \widehat{\mathcal{J}}_0^c(w)} \left(\frac{\varphi'(\|G_j \hat{u}\|_2)}{\|G_j \hat{u}\|_2} \frac{\|G_j w\|_2^2 \|G_j \hat{u}\|_2^2}{\langle G_j \hat{u}, G_j w \rangle^2} - \frac{\varphi'(\|G_j \hat{u}\|_2)}{\|G_j \hat{u}\|_2} \right) \left(\frac{\langle G_j \hat{u}, G_j w \rangle}{\|G_j \hat{u}\|_2} \right)^2 \\
 \text{by (a)} &\leq \beta \sum_{j \in \widehat{\mathcal{J}}_0^c(w)} \left(\varphi''(\|G_j \hat{u}\|_2) + \frac{\varphi'(\|G_j \hat{u}\|_2)}{\|G_j \hat{u}\|_2} (C - 1) \right) \left(\frac{\langle G_j \hat{u}, G_j w \rangle}{\|G_j \hat{u}\|_2} \right)^2 \\
 \text{by (b)} &< 0 \quad \forall w \in K_{\hat{u}} \setminus \{0\}.
 \end{aligned}$$

The proof is complete. \square

Below we discuss the additional assumption (b) in Lemma 5.

Remark 5. The inequality required in (b) can be controlled using the parameter α used to define φ (see Table 1). For instance, if $C = 2$, the assumption is satisfied by the PF (f1) in Table 1 for $t \geq \tau_0 > 1/\alpha$ and by the PF (f2) for $t \geq \tau_0 > 1/(-\ln \alpha) > 0$. These PFs are bounded above. This assumption is satisfied by the PFs (f3) for $t \leq \tau_1 < 1 - 1/\alpha$ and by (f4) for $t \leq \tau_1 < (1/1 - \alpha)^{1/\alpha}$.

PROPOSITION 3. Consider \mathcal{F} as given in (6) where H2 is verified. Let \hat{u} be such that $\widehat{\mathcal{J}}_0 \neq \emptyset$ and H3 holds true. If $\{G_j\}$ contains some matrices $G_j \in \mathbb{R}^{s \times p}$ for $s \geq 2$, we also adopt assumptions (a)–(b) in Lemma 5. Suppose that

$$(30) \quad \dim K_{\hat{u}} \geq 1,$$

where $K_{\hat{u}}$ reads according to (24). Then \hat{u} is not a (local) minimizer of \mathcal{F} .

Proof. The proof of the proposition is conducted by contradiction. So suppose that

$$(31) \quad \hat{u} \text{ is a (local) minimizer of } \mathcal{F}.$$

The cost function \mathcal{F} in (6) can be rewritten as

$$(32) \quad \mathcal{F}(\hat{u}) = \sum_{i \in \widehat{\mathcal{I}}_0} |a_i \hat{u} - v[i]| + \beta \sum_{i \in \widehat{\mathcal{J}}_0} \varphi(\|G_i \hat{u}\|_2) + F(\hat{u}),$$

where $F \stackrel{\text{def}}{=} \mathcal{F}|_{\mathcal{K}_{\hat{u}}}$. The first two sums in the equation above are null, so

$$\mathcal{F}(\hat{u}) = F(\hat{u}).$$

From the definition of $K_{\hat{u}}$ in (24), we have

$$(33) \quad w \in K_{\hat{u}} \Rightarrow \begin{cases} a_i(\hat{u} + w) = a_i \hat{u} = v[i] & \forall i \in \widehat{\mathcal{I}}_0, \\ \|G_j(\hat{u} + w)\|_2 = \|G_j \hat{u}\|_2 = 0 & \forall j \in \widehat{\mathcal{J}}_0. \end{cases}$$

Hence,

$$(34) \quad \begin{aligned} w \in K_{\hat{u}} \Rightarrow \mathcal{F}(\hat{u} + w) &= \sum_{i \in \hat{I}_0^c} |a_i(\hat{u} + w) - v[i]| + \beta \sum_{i \in \hat{J}_0^c} \varphi(\|G_i(\hat{u} + w)\|_2) \\ &= F(\hat{u} + w). \end{aligned}$$

Since \mathcal{F} has a (local) minimum at \hat{u} by (31), there is $\rho > 0$ such that

$$w \in K_{\hat{u}} \cap B(0, \rho) \Rightarrow \mathcal{F}(\hat{u}) \leq \mathcal{F}(\hat{u} + w).$$

Combining this with (34) yields

$$(35) \quad w \in K_{\hat{u}} \cap B(0, \rho) \Rightarrow F(\hat{u}) = \mathcal{F}(\hat{u}) \leq \mathcal{F}(\hat{u} + w) = F(\hat{u} + w).$$

Hence F should have a (local) minimum at \hat{u} and should in particular satisfy the second-order necessary condition for a (local) minimum⁷ $\langle D^2F(\hat{u})w, w \rangle \geq 0$ for all $w \in K_{\hat{u}}$. However, Lemmas 4 and 5 tell us that if (30) holds, then \hat{u} is *not* a (local) minimizer of F because

$$(36) \quad \langle D^2F(\hat{u})w, w \rangle < 0 \quad \forall w \in K_{\hat{u}} \setminus \{0\}.$$

Hence (31) is false, which proves the statement of the proposition. □

Now we can draw an important conclusion.

Remark 6. According to Proposition 2, any minimizer \hat{u} of \mathcal{F} in (6) belongs to a nonempty manifold of the form $\mathcal{K}_{\hat{u}}$, as given in (23). All points \hat{u} described in Proposition 3 belong to nonempty manifolds of the form $\mathcal{K}_{\hat{u}}$; however, *they are not (local) minimizers of \mathcal{F}* . The reason is that the vector space $K_{\hat{u}}$, tangent to $\mathcal{K}_{\hat{u}}$, meets $\dim K_{\hat{u}} \geq 1$.

2.4. The (local) minimizers of \mathcal{F} : Exact fitting results. From Proposition 1 we know that \mathcal{F} has minimizers. Based on Remark 6, one can guess that if \hat{u} is a (local) minimizer of \mathcal{F} , then the relevant vector subspace $K_{\hat{u}}$ has a null dimension. This is made explicit in the theorem below.

THEOREM 1. *Consider \mathcal{F} , as given in (6), satisfying H1 and H2. Let \hat{u} be a (local) minimizer of \mathcal{F} meeting $\hat{J}_0^c \neq \emptyset$ and H3. If $\{G_j\}$ contains some matrices $G_j \in \mathbb{R}^{s \times p}$ for $s \geq 2$, we also assume (a)–(b) in Lemma 5. Then*

- (i) $\mathcal{K}_{\hat{u}} = \{\hat{u}\}$ and $K_{\hat{u}} = \{0\}$, where $\mathcal{K}_{\hat{u}}$ and $K_{\hat{u}}$ read according to (23) and (24), respectively.
- (ii) \hat{u} is the unique solution of the full column rank linear system given by

$$(37) \quad \begin{cases} a_i w = v[i] & \forall i \in \hat{I}_0, \\ G_j w = 0 & \forall j \in \hat{J}_0. \end{cases}$$

Proof. Since \hat{u} is a (local) minimizer of \mathcal{F} , it follows from Proposition 3 that⁸ $\dim K_{\hat{u}} = 0$, and hence

$$(38) \quad K_{\hat{u}} = \{0\}$$

⁷It may be useful to recall that F is C^2 near \hat{u} according to Lemma 1.

⁸Indeed, (35) and (36) show that the only possibility for \hat{u} to be a (local) minimizer of \mathcal{F} is that $w = 0$ for all $w \in K_{\hat{u}}$.

(recall that $K_{\hat{u}}$ is a vector subspace of \mathbb{R}^p). Substituting (38) into (25) shows that

$$\mathcal{K}_{\hat{u}} = \{\hat{u}\}.$$

Thus claim (i) is proven.

Let the components of \hat{I}_0 and \hat{J}_0 read as

$$\hat{I}_0 = \{i_1, \dots, i_{\#\hat{I}_0}\} \quad \text{and} \quad \hat{J}_0 = \{j_1, \dots, j_{\#\hat{J}_0}\}.$$

Define the following p -column matrices:

$$A_0 = \begin{bmatrix} a_{i_1} \\ \vdots \\ a_{\#\hat{I}_0} \end{bmatrix} \quad \text{and} \quad G_0 = \begin{bmatrix} G_{j_1} \\ \vdots \\ G_{\#\hat{J}_0} \end{bmatrix}$$

as well as

$$(39) \quad H_0 = \begin{bmatrix} A_0 \\ G_0 \end{bmatrix}.$$

Using the definition of $K_{\hat{u}}$ in (24) along with the result in (38) shows that

$$(40) \quad \{0\} = K_{\hat{u}} = \{w \in \mathbb{R}^p \mid H_0 w = 0\} = \ker H_0.$$

Hence

$$\text{rank } H_0 = p.$$

Define also the column vector v_0 by

$$v_0 = [v[i_1], \dots, v[\#\hat{I}_0], \mathbb{O}_m^T]^T,$$

where m is the number of rows in G_0 (e.g., $m = \#\hat{J}_0$ if $s = 1$) and \mathbb{O}_m is the m -length column vector composed of zeros. Consequently, \hat{u} is the unique solution of the matrix equation given by

$$(41) \quad H_0 w = v_0.$$

This equation is the same as (37). This establishes (ii). □

A significant outcome of Theorem 1 is formulated next.

Remark 7. Theorem 1 furnishes an important *necessary condition* for a (local) minimizer \hat{u} of \mathcal{F} : the corresponding linear system in (37) must have *full column rank*.

The examples below illustrate Theorem 1.

Example 4. Let us focus yet again on Example 2. From the ingredients of \mathcal{F} given in (11), the minimizer in (12), and the relevant \hat{I}_0 and \hat{J}_0 described in (14), the set $\mathcal{K}_{\hat{u}}$ satisfies

$$\begin{aligned} \mathcal{K}_{\hat{u}} &= \{w \in \mathbb{R}^3 \mid a_1 w = v[1], a_2 w = v[2], g_1 w = 0\} \\ &= \{w \in \mathbb{R}^3 \mid w[1] = v[1], w[3] = v[2], w[1] - w[2] = 0\} \\ &= \{w \in \mathbb{R}^3 \mid w[1] = v[1], w[3] = v[2], w[2] = w[1]\} \\ &= \{w \in \mathbb{R}^3 \mid w[1] = w[2] = v[1], w[3] = v[2]\} \\ &= \{w \in \mathbb{R}^3 \mid w[1] = 1, w[2] = 1, w[3] = 3\} \\ &= \{\hat{u}\}. \end{aligned}$$

Then $K_{\hat{u}} = \{0\}$. Furthermore, the linear system defined according to (37) has a unique solution. Indeed, the corresponding matrix H_0 (see (39)) reads

$$H_0 = \begin{bmatrix} 1 & 0 & 0 \\ 0 & 0 & 1 \\ 1 & -1 & 0 \end{bmatrix}.$$

Clearly, H_0 has full column rank since $\text{rank } H_0 = 3$.

Example 5. The data vector v in Figure 2 is of length 80. One can check that the minimizer depicted in Figure 2(b) satisfies

$$\widehat{I}_0^c = (28, 29, 30, 31, 69, 70) \quad \text{and} \quad \widehat{J}_0^c = (4, 20, 44, 59).$$

Then the corresponding matrix H_0 is of size 149×80 . It satisfies $\text{rank } H_0 = 80$.

We can now formulate an important *practical* conclusion: each pixel of a (local) minimizer \hat{u} of \mathcal{F} is involved in (at least) one data equation that is fitted exactly, $a_i \hat{u} = v[i]$, or in (at least) one vanishing differential operator, $\|G_j \hat{u}\|_2 = 0$, or in both types of equations. The formal statement of this is given next.

THEOREM 2. *Consider \mathcal{F} , as given in (6), satisfying H1 and H2. For $v \in \mathbb{R}^q \setminus \{0\}$, let \hat{u} be a (local) minimizer of \mathcal{F} meeting $\widehat{J}_0^c \neq \emptyset$ and H3. If $\{G_j\}$ contains some matrices $G_j \in \mathbb{R}^{s \times p}$ for $s \geq 2$, then (a)–(b) in Lemma 5 are assumed as well. Then*

$$(42) \quad 1 \leq k \leq p \Rightarrow \begin{cases} \exists i \in I \text{ obeying } a_i \hat{u} = v[i] & \text{such that } a_i[k] \neq 0, \\ & \text{or} \\ \exists j \in J \text{ obeying } G_j \hat{u} = 0 & \text{such that } G_j(k) \neq 0, \end{cases}$$

where $G_j(k) \in \mathbb{R}^s$ is the k th column of the matrix $G_j \in \mathbb{R}^{s \times p}$.

Proof. For \hat{u} , let \widehat{I}_0 and \widehat{J}_0 be defined according to (13). Then (42) is equivalent to

$$(43) \quad 1 \leq k \leq p \Rightarrow \begin{cases} \exists i \in \widehat{I}_0 & \text{such that } a_i[k] \neq 0, \\ & \text{or} \\ \exists j \in \widehat{J}_0 & \text{such that } G_j(k) \neq 0. \end{cases}$$

We shall prove (43) by contradiction. So suppose that there is a $k \in \{1, \dots, p\}$ such that

$$(44) \quad \begin{cases} a_i[k] = 0 & \forall i \in \widehat{I}_0, \\ G_j(k) = 0 & \forall j \in \widehat{J}_0. \end{cases}$$

Then the k th column of the matrix H_0 in (39) is null; hence (40) fails to hold. This entails that the vector subspace $K_{\hat{u}}$, defined according to (24), satisfies

$$\dim K_{\hat{u}} \geq 1.$$

Then Proposition 3 tells us that \hat{u} is not a (local) minimizer of \mathcal{F} . This conclusion contradicts the fact that \hat{u} is a (local) minimizer of \mathcal{F} . Hence the assumption in (44) is false. Consequently, (43) and the statement of the theorem (42) hold true. \square

In the simple case when $A = I$ and $\{G_j\}$ yield either discrete gradients or first-order finite differences between adjacent samples, the result stated in (42) means that

a (local) minimizer is composed partly of constant patches and partly of pixels that fit data samples exactly, as seen, e.g., in Figures 2 and 3.

Remark 8 (on the role of the regularization parameter $\beta > 0$). The linear system in (37) that a (local) minimizer \hat{u} of \mathcal{F} solves (Theorem 1) does not make an explicit reference to the regularization parameter β . Implicitly, β helps the selection of the subsets \hat{I}_0 and \hat{J}_0 in (37). Usually \mathcal{F} has numerous (local) minimizers. According to the same theorem, each one of them is the unique solution of a linear system of the form given there. Any other (local) minimizer \hat{u}' corresponds to different subsets $\hat{I}'_0 \subset I$ and $\hat{J}'_0 \subset J$ and, in general, $\mathcal{F}(\hat{u}) \neq \mathcal{F}(\hat{u}')$. So the ordering of the (local) minimizers \hat{u} of \mathcal{F} according to their value $\mathcal{F}(\hat{u})$, as well as the selection of the global minimizer of \mathcal{F} , are controlled by β .

3. Minimization method.

3.1. A continuation approach. The minimization of nonconvex nonsmooth cost function \mathcal{F} of the form (6) involves several intrinsic difficulties that drastically restrict the numerical methods that can be envisaged. Since φ is concave, \mathcal{F} typically exhibits a certain number of local minima which are not global. What is more, Theorem 1 in section 2 tells us that at any (local) minimizer \hat{u} , \mathcal{F} is nonsmooth in all directions in \mathbb{R}^p . Thus usual gradient-based methods are inappropriate even for local minimization. Note also that often the matrix A has numerous off-diagonal nonzero elements and is ill-conditioned, which is a hard test for any numerical scheme. In [35, 36], a nonsmooth continuation GNC⁹-like approach was proposed to minimize cost functions combining an ℓ_2 quadratic data fitting and regularization defined using concave functions φ in our cost function \mathcal{F} in (6). The experimental results there showed that the resultant numerical method provides better performance with significantly lower computational cost compared to stochastic algorithms such as simulated annealing. We shall apply a similar nonsmooth continuation idea to dealing with both nonsmooth terms of our cost functions \mathcal{F} in (6).

The concave function φ can be approximated by a family of functions $\varphi_\varepsilon : \mathbb{R}_+ \rightarrow \mathbb{R}_+$, parameterized by $\varepsilon \in [0, 1]$, so that φ_0 is convex, φ_ε continuously goes to φ as ε increases from 0 to 1, and $\varphi_1 = \varphi$. Correspondingly, the cost function \mathcal{F} is approximated by a family \mathcal{F}_ε given by

$$(45) \quad \mathcal{F}_\varepsilon(u) = \|Au - v\|_1 + \beta \sum_{j \in J} \varphi_\varepsilon(\|G_j u\|_2), \quad \varepsilon \in [0, 1].$$

Thus \mathcal{F}_0 is convex, \mathcal{F}_ε continuously goes to \mathcal{F} when ε increases from 0 to 1, and we have $\mathcal{F}_1 = \mathcal{F}$. The main heuristic behind continuation [44] is that if $u^{(0)}$ minimizes the convex \mathcal{F}_1 , the family of *local* minimizers $u^{(\varepsilon)}$ of \mathcal{F}_ε converges to a good approximation of the global minimizer of the original $\mathcal{F} = \mathcal{F}_1$ as ε increases. Thus a reasonable requirement is that the approximations φ_ε share the same features as the original φ : so φ_ε shall be constructed so that

$$(46) \quad \varphi_\varepsilon \text{ satisfy assumption H2 } \forall \varepsilon \in (0, 1] \text{ and } \varphi_0(t) = t.$$

So φ_ε are concave for every $\varepsilon \in (0, 1]$, and $\varphi''_\varepsilon(t) < 0$ continuously decreases towards $\varphi''(t) < 0$ for every $t \in \mathbb{R}_+$. Since φ_ε meets H2, each φ_ε can be decomposed as

$$(47) \quad \varphi_\varepsilon(t) = \psi_\varepsilon(t) + \alpha_\varepsilon t, \quad \text{where } \alpha_\varepsilon = \varphi'_\varepsilon(0^+).$$

⁹GNC stands for graduated nonconvexity, a method proposed by Blake and Zisserman [7] for solving computer vision problems (where $A = I$) using the discrete version of the Mumford-Shah functional.

Then \mathcal{F}_ε in (45) equivalently reads¹⁰

$$(48) \quad \mathcal{F}_\varepsilon(u) = \|Au - v\|_1 + \beta\alpha_\varepsilon \sum_{j \in J} \|G_j u\|_2 + \beta\Psi_\varepsilon(u),$$

$$\text{where } \Psi_\varepsilon(u) = \sum_{j \in J} \psi_\varepsilon(\|G_j u\|_2).$$

This formulation of \mathcal{F}_ε can be handled more easily than the one in (45):

- The first two terms in (48) are convex and nondifferentiable;
- Ψ_ε is nonconvex (ψ_ε in (47) is the difference between a nonconvex function and a linear function), and it is differentiable on \mathbb{R}^p because $\psi'_\varepsilon(0^+) = 0$ and $\lim_{t \searrow 0} \frac{\psi'_\varepsilon(t)}{t}$ is finite by assumption H2.

In practice, a strictly increasing sequence

$$(49) \quad \varepsilon_0 = 0 < \varepsilon_1 < \dots < \varepsilon_k < \dots < \varepsilon_n = 1$$

is selected, and for any $k \in \{1, \dots, n\}$ one computes the minimizer $u^{(k)}$ of the corresponding $\mathcal{F}_{\varepsilon_k}$, which is initialized with the previously obtained $u^{(k-1)}$.

To simplify the notation, we shall write ε for ε_k whenever this is clear from the context.

3.2. Penalization scheme to fit $\|Au - v\|_1$ and $\|Gu\|_2$. In this subsection, we develop a numerical method to minimize \mathcal{F}_ε in (48) for every $\varepsilon \in [0, 1]$. It is based on variable-splitting and penalty techniques. The idea is to transfer the nonsmooth terms $\|Au - v\|_1$ and $\|Gu\|_2$ out of \mathcal{F}_ε in such a way that the minimization steps relevant to these convex nonsmooth terms can be done using shrinkage operations, as proposed in [47]. To this end, we consider an augmented cost function $\mathcal{J}_{\varepsilon,\gamma} : \mathbb{R}^p \times \mathbb{R}^q \times \mathbb{R}^{sp} \rightarrow \mathbb{R}$ which involves a fitting of the auxiliary variables $z \in \mathbb{R}^{sp}$ and $w \in \mathbb{R}^q$ to Gu and to Au , respectively, weighted by a penalty parameter $\gamma > 0$:

$$(50) \quad \mathcal{J}_{\varepsilon,\gamma}(u, w, z) = \gamma\|Au - w\|_2^2 + \|w - v\|_1 + \beta\Psi_\varepsilon(u) + \gamma\|Gu - z\|_2^2 + \beta\alpha_\varepsilon \sum_{j \in J} \|z_j\|_2.$$

Clearly, $z_j \in \mathbb{R}^s$ for all $j \in J$. For any $\varepsilon \in [0, 1]$, we propose an iterative algorithm where γ is increased progressively. Indeed,

$$\lim_{\gamma \rightarrow \infty} \mathcal{J}_{\varepsilon,\gamma}(u, w, z) = \mathcal{F}_\varepsilon(u) \quad \forall \varepsilon \in [0, 1],$$

where $\mathcal{F}_\varepsilon(u)$ reads as in (48). When γ is large enough, we have $w \approx Au$ and $z \approx Gu$.

For u and w fixed, the function $z \mapsto \mathcal{J}_{\varepsilon,\gamma}(u, w, z)$ is convex and nondifferentiable because of the term $\sum_j \|z_j\|_2$. For u and z fixed, $w \mapsto \mathcal{J}_{\varepsilon,\gamma}(u, w, z)$ is convex and nondifferentiable because of the term $\|w - v\|_1$. Given w and z , the function $u \mapsto \mathcal{J}_{\varepsilon,\gamma}(u, w, z)$ is twice differentiable and nonconvex so that it can be minimized by

¹⁰Note that according to (46) we have the implication $[\psi_0(t) = 0 \Rightarrow \Psi_0(u) = 0]$.

gradient-based methods. The computational steps are given as follows:

$$\begin{aligned}
 z^{(l,k)} &= \arg \min_{z \in \mathbb{R}^{sp}} \mathcal{J}_{\varepsilon, \gamma}(u^{(l-1,k)}, w^{(l-1,k)}, z) \\
 (51) \quad &= \arg \min_{z \in \mathbb{R}^{sp}} \left\{ \sum_{j \in J} \left(\gamma \|G_j u^{(l-1,k)} - z_j\|_2^2 + \beta \alpha_\varepsilon \|z_j\|_2 \right) \right\},
 \end{aligned}$$

$$\begin{aligned}
 w^{(l,k)} &= \arg \min_{w \in \mathbb{R}^q} \mathcal{J}_{\varepsilon, \gamma}(u^{(l-1,k)}, w, z^{(l,k)}) \\
 (52) \quad &= \arg \min_{w \in \mathbb{R}^q} \left\{ \gamma \|Au^{(l-1,k)} - w\|_2^2 + \|w - v\|_1 \right\},
 \end{aligned}$$

$$\begin{aligned}
 u^{(l,k)} &= \arg \min_{u \in \mathbb{R}^p} \mathcal{J}_{\varepsilon, \gamma}(u, w^{(l,k)}, z^{(l,k)}) \\
 (53) \quad &= \arg \min_{u \in \mathbb{R}^p} \left\{ \gamma \|Au - w^{(l,k)}\|_2^2 + \gamma \|Gu - z^{(l,k)}\|_2^2 + \beta \Psi_\varepsilon(u) \right\}.
 \end{aligned}$$

In this case, we initialize with $u^{(0,k)} \stackrel{\text{def}}{=} u_{\varepsilon_{k-1}}$, where $u_{\varepsilon_{k-1}}$ results from the minimization of $\mathcal{J}_{\varepsilon_{k-1}}$ with respect to u . We remark that $w^{(l-1,k)}$ is not required in the computation in (51). Problems (52) and (53) will be solved in an exact and fast way using multidimensional shrinkage¹¹ according to [47, p. 577].

Computation of $z^{(l,k)}$ according to (51). Solving (51) amounts to solving p independent problems:

$$(54) \quad z_i^{(l,k)} = \arg \min_{z_j \in \mathbb{R}^s} \left\{ \gamma \|G_j u^{(l-1,k)} - z_j\|_2^2 + \beta \alpha_\varepsilon \|z_j\|_2 \right\} \quad \forall i \in J.$$

As shown in [47, p. 577] (see also the footnote below), each one of the problems in (54) can be solved efficiently using s -dimensional shrinkage:

$$(55) \quad z_i^{(l,k)} = \frac{G_i u^{(l-1,k)}}{\|G_i u^{(l-1,k)}\|_2} \max \left\{ \|G_i u^{(l-1,k)}\|_2 - \frac{\beta \alpha_\varepsilon}{2\gamma}, 0 \right\} \quad \forall i \in J.$$

Computation of $w^{(l,k)}$ according to (52). The task is similar to the computation of $z^{(l,k)}$. The solution in (52) can be found (see footnote below):

$$(56) \quad w_i^{(l,k)} = \frac{Au^{(l-1,k)} - v}{\|Au^{(l-1,k)} - v\|_2} \max \left\{ \|Au^{(l-1,k)} - v\|_2 - \frac{1}{2\gamma}, 0 \right\} \quad \forall i \in I.$$

Computation of $u^{(l,k)}$ according to (53). For $\varepsilon_0 = 0$, the finding of $u^{(l,0)}$ amounts to minimizing the convex quadratic function:

$$\min_{u \in \mathbb{R}^p} \left\{ \gamma \|Au - w^{(l,0)}\|_2^2 + \gamma \|Gu - z^{(l,0)}\|_2^2 \right\}.$$

For $\varepsilon > 0$, a quasi-Newton method shall be used to solve (53). The gradient vector $\nabla_u \mathcal{J}_{\varepsilon, \gamma} \stackrel{\text{def}}{=} \nabla_u \mathcal{J}_{\varepsilon, \gamma}(u, w^{(l,k)}, z^{(l,k)})$ as well as the Hessian matrix $\nabla_u^2 \mathcal{J}_{\varepsilon, \gamma} \stackrel{\text{def}}{=} \nabla_u^2 \mathcal{J}_{\varepsilon, \gamma}(u, w^{(l,k)}, z^{(l,k)})$ of the function $u \mapsto \mathcal{J}_{\varepsilon, \gamma}(u, w^{(l,k)}, z^{(l,k)})$ read

$$(57) \quad \nabla_u \mathcal{J}_{\varepsilon, \gamma} = 2\gamma A^T (Au - w^{(l,k)}) + 2\gamma (G^T Gu - z^{(l,k)}) + \beta \nabla_u \Psi_{\varepsilon_k}(u),$$

$$(58) \quad \nabla_u^2 \mathcal{J}_{\varepsilon, \gamma} = 2\gamma A^T A + 2\gamma G^T G + \beta \nabla_u^2 \Psi_{\varepsilon_k}(u).$$

¹¹Let $(x, y) \in \mathbb{R}^n \times \mathbb{R}^n$ for any integer $n \geq 1$ and $\kappa > 0$. The multidimensional shrinkage formula reads $\arg \min_{x \in \mathbb{R}^n} (\|x\|_2 + \kappa \|x - y\|_2^2) = \max \left\{ \|y\|_2 - \frac{1}{2\kappa}, 0 \right\} \frac{y}{\|y\|_2}$.

Since $\nabla_u^2 \Psi_\varepsilon(u)$ is negative definite for $\varepsilon \in (0, 1]$, the Hessian $\nabla_u^2 \mathcal{J}_{\varepsilon, \gamma}$ may not be positive definite. This may prevent the quasi-Newton method from converging, as the resultant search direction may not be a descent direction. We can obtain a descent direction by using only the positive definite part of the Hessian matrix in the minimization procedure. Thanks to H1, the coefficient matrix $2\gamma A^T A + 2\gamma G^T G$ is always positive definite. The solution can then be updated according to

$$u^{(l,k)} = u^{(l-1,k)} + \tau \Delta u^{(l,k)},$$

where $\tau > 0$ is the step-size and $\Delta u^{(l,k)}$ is found by solving

$$(59) \quad (2\gamma A^T A + 2\gamma G^T G) \Delta u^{(l,k)} = -\nabla_u \mathcal{J}_{\varepsilon, \gamma}.$$

In image restoration problems A is often a blurring matrix generated by a symmetric point spread function. Then the computational cost of the method is dominated by three fast discrete transforms in solving the linear system in (59); see [30]. The computational cost for each fast transform is only $O(p \log p)$ for a $p \times p$ blurring matrix A [30].

Three strategies to determine the step-size τ were tested: the Armijo rule, the Goldstein rule, and a fixed τ [37, Chapter 3]. The experimental results have shown that the numerical schemes based on these three rules converge to the same solution, but the use of the first two rules requires a heavy additional computation cost. Therefore, we fixed $\tau = 1$ in all our experiments.

3.3. Algorithm.

Set $\varepsilon_0 = 0$ and $\Delta\varepsilon = 1/n$, and initialize $u^{(0,0)}$.

For $k = 0 \rightarrow n$,

Set $l = 1$, initial value of γ , and $\text{relerr} = \text{tol} + 1$.

While $\text{relerr} > \text{tol}$ do

Obtain $z^{(l,k)}$ by computing (55) and $w^{(l,k)}$ by computing (56);

If $k = 0$,

Solve $(2\gamma A^T A + 2\gamma \sum_{j \in J} G_j^T G_j) u^{(l,k)} = A^T w^{(l,k)} +$

$\gamma \sum_{j \in J} G_j^T z^{(l,k)}$;

Otherwise

Solve $(2\gamma A^T A + 2\gamma \sum_{j \in J} G_j^T G_j) \Delta u^{(l,k)} = -\nabla_u \mathcal{J}_{\varepsilon_k}$;

Update $u^{(l,k)} = u^{(l-1,k)} + \tau \Delta u^{(l,k)}$;

End If;

Compute $\text{relerr} = \|u^{(l,k)} - u^{(l-1,k)}\|_2 / \|u^{(l,k)}\|_2$;

End While.

Increase γ (e.g., by multiplying γ with a factor greater than 1) and set

$l = l + 1$;

Set $u^{(0,k+1)} = u^{(l,k)}$ (for the initial guess of the next outer loop);

Update $\varepsilon_{k+1} = \varepsilon_k + \Delta\varepsilon$;

End For.

In the next section, we will test the performance of the proposed method for different imaging problems.

4. Numerical experiments. We shall present the experimental results in high-resolution image reconstruction [29], magnetic resonance (MR) image reconstruction from highly undersampled noisy data, and deblurring under impulse noise to test the effectiveness of the proposed algorithm as well as the possibilities offered by the

family of cost functions in (6) satisfying assumption H2. All original images used in our experiments are normalized in the range between 0 and 1. Peak signal-to-noise ratio¹² (PSNR) is used to evaluate the quality of the recovered images, while CPU time is also used to evaluate the efficiency of the method. The parameter tol is set to be 10^{-4} in the proposed algorithm. The initial value of γ is set to 0.1, and its value is updated by 1.2γ at each iteration. The PF used in all the illustrations is (f1) in Table 1, and our choice for φ_ε is

$$(60) \quad \varphi_\varepsilon(t) = \frac{\alpha t}{1 + \varepsilon \alpha t}, \quad 0 \leq \varepsilon \leq 1.$$

As required in subsection 3.1, φ_ε satisfies assumption H2 for any $\varepsilon \in (0, 1]$. It is obvious that φ_0 is convex and that $\varphi_1 = \varphi$. By (60), we have $\alpha_\varepsilon = \alpha$ for any $\varepsilon \in (0, 1]$. In the tests, we use $\alpha \in \{0.5, 1\}$.

All the computational tasks are performed using MATLAB on a computer with Corel2 CPU with 2.66 GHz and 1.98GB of RAM.

In what follows, our method—the minimization of \mathcal{F} in (6) using the numerical scheme proposed in section 3.3—is compared to other variational image reconstruction methods. *Systematically, for all competing methods and for each data set, the parameter values are selected manually to reach the best performance level in terms of PSNR.*

4.1. High-resolution image reconstruction. In the first experiment, we use the proposed algorithm to generate a high-resolution image from a low-resolution image. The aim is to demonstrate that the pixel value of a high-resolution image can fit the pixel value of a low-resolution image exactly at the same location. The original image—the picture of Lena of size 256×256 —and the low-resolution 128×128 observed image v are as shown in Figure 6 (top row). The data image v is generated from the original image by downsampling of factor 2, and its gray values are rescaled in $[0, 1]$. Two restorations \hat{u} based on the low-resolution 128×128 image v are shown in the bottom row in Figure 6. Let \hat{u}_J denote the subset of all 128^2 restored pixels that correspond to the data pixels v . The bicubic method does not fit data samples correctly, since $\text{mean}(\hat{u}_J - v) = 1.8 \times 10^{-2}$ and $\|\hat{u}_J - v\|_\infty = 2.6 \times 10^{-1}$. We applied our algorithm to minimize \mathcal{F} in (6) where all operators $\{G_j\}$ correspond to the discrete form of the Laplacian operator given by

$$(61) \quad \begin{bmatrix} 0 & -1 & 0 \\ -1 & 4 & -1 \\ 0 & -1 & 0 \end{bmatrix}.$$

All data pixels are fitted with a remarkable numerical precision since $\text{mean}(\hat{u}_J - v) = 1.7 \times 10^{-6}$ and $\|\hat{u}_J - v\|_\infty = 3.6 \times 10^{-5}$, which matches the precision given by the parameter tol . This result corroborates with the theory in section 2.

4.2. MR image reconstruction from highly undersampled data. Our goal is to explore the ability of the proposed method to solve highly underdetermined, ill-posed inverse problems when relevant prior on the sought-after solution is available. We focus on MR image recovery from a very few samples in the k -space (i.e., individual noisy Fourier coefficients). This problem can be related to compressed sensing in MRI; see, e.g., [26, 27].

¹²Noticing that our original images are normalized on $[0, 1]$, the $\text{PSNR} = 10 \log_{10} \frac{p}{\|\hat{u} - u_o\|_2^2}$, where u_o is the original image and p is the number of pixels that it contains.



The original image
256 × 256



Low-resolution 128 × 128 data v ,
 $v[i, j] \in [0, 1], \forall (i, j) \in J$



Bicubic method
 $\text{mean}(\hat{u}_J - v) = 1.8 \times 10^{-2}$
 $\|\hat{u}_J - v\|_\infty = 2.6 \times 10^{-1}$
PSNR = 26.11dB



The proposed method
 $\text{mean}(\hat{u}_J - v) = 1.7 \times 10^{-6}$
 $\|\hat{u}_J - v\|_\infty = 3.6 \times 10^{-5}$
PSNR = 28.93dB

FIG. 6. *High-resolution image reconstruction. In our method, the operators $\{G_j\}$ correspond to the discrete Laplacian operator in (61); data samples are fitted with a remarkable numerical precision. This clearly does not hold for the bicubic method.*

Experiments are done with the 128 × 128 Shepp–Logan phantom in Figure 7, normalized on $[0, 1]$.

Two data vectors are considered: they contain only 7% and 5% *randomly* chosen samples in the k -space, contaminated with SNR = 37 dB white centered *Gaussian* noise.

The Shepp–Logan phantom being locally constant with oval shapes, the linear operators $\{G_j\}$ in our cost function (6) yield the usual discrete gradient of the image,¹³ so that the regularization term provides a correct prior. Indeed, $G u_{\text{original}}$ is the sparsest linear transform for this image, the PFs in our cost function (6) promote sparsity in this transformed domain, and the terms $G_j u$ are rotation invariant (in a discrete sense). Clearly, A is the undersampled Fourier transform corresponding to

¹³In other words, each G_j is a $2 \times p$ matrix for p the number of pixels, along with appropriate boundary conditions. The potential function φ —(f1) in Table 1—is applied to $\|G_j u\|_2$ for all $j \in J$.

FIG. 7. Original image: the Shepp-Logan phantom with gray-scale range in $[0, 1]$.

TABLE 2

PSNR and CPU time for our method applied to the 7% data vector as a function of the value of the parameter β .

β	PSNR (dB)	CPU time (seconds)
2.19×10^{-6}	14.45	12.61
4.38×10^{-6}	15.33	26.73
8.75×10^{-6}	16.94	39.38
1.75×10^{-5}	20.24	49.27
3.50×10^{-5}	26.22	49.86
7.00×10^{-4}	75.64	48.94
1.40×10^{-4}	71.52	36.33
2.80×10^{-4}	21.20	97.11
5.60×10^{-4}	13.44	1.22
1.12×10^{-3}	13.44	1.11
2.24×10^{-3}	13.44	1.14

the 7% or 5% randomly chosen k -samples.

Table 2 shows the PSNR and the computational time to run our algorithm (see section 3.3) for the first data set (7% random noisy samples) for different values of β . One observes that the highest PSNR is obtained for $\beta = 7.00 \times 10^{-4}$, which requires nearly 49 seconds. The best CPU time—1.11 seconds—corresponds to $\beta = 1.12 \times 10^{-3}$, but the PSNR is the worst.

Our method—the minimization of \mathcal{F} in (6) using the numerical scheme proposed in section 3.3—is compared to four other variational image reconstruction methods. In all cases, A is as described above, and regularization is applied to the discrete gradient of the image, as in our method.

ℓ_1 -NN via e-BFGS. Recently the BFGS (Broyden-Fletcher-Goldfarb-Shanno) minimization method was extended in [23] to handle nonsmooth, not necessarily convex problems (called e-BFGS). We applied this e-BFGS numerical scheme to minimize the ℓ_1 -nonsmooth nonconvex cost function \mathcal{F} proposed in (6). To this end we used the MATLAB package HANSO developed by the authors and freely available.¹⁴

ℓ_2 -TV. For Gaussian noise, an ℓ_2 quadratic data fitting term is a classical choice.¹⁵ TV regularization—see (4)—is well known to give rise to images containing constant regions with edges. The ℓ_2 -TV cost function

$$(62) \quad \|Au - v\|_2^2 + \beta \text{TV}(u)$$

¹⁴See <http://www.cs.nyu.edu/overton/software/hanso/>.

¹⁵This choice is well justified in a statistical framework.

is a common tool for solving various image reconstruction problems; see, e.g., the textbook [2]. Let us notice that ℓ_2 -TV is a typical ingredient in compressed sensing MRI reconstruction [27]. The solution was computed using the alternating minimization algorithm conceived in [43].

ℓ_1 -TV. Some MR image registration problems have been successfully solved using an ℓ_1 -TV cost function; see, e.g., [38, 21]. We will test this cost function for our MRI problem as far as it can be seen as a predecessor of the cost functions we propose in this paper. The numerical results are obtained using the method described¹⁶ in [20].

ℓ_2 -NN. Since [16, 17], nonsmooth nonconvex cost functions composed of an ℓ_2 quadratic data fitting term, as in (62), and a regularization term, as in (6), for φ the function (f1) in Table 1 have been successfully used to solve various ill-posed inverse problems. In our experiments, the global minimizer is approximated using the recent Algorithm II in [36, pp. 3079–3080].

For each data vector, all numerical schemes were initialized using the corresponding zero-filling Fourier reconstruction. Note that the latter contains normal random noise, so it satisfies the initialization requirements for the e-BFGS method [23]. We also tried purely random initializations for both data vectors: ℓ_1 -NN via e-BFGS converged to meaningless solutions, which are not shown.

The reconstruction results based on the 7% data vector are depicted in Figure 8, and the relevant PSNR values and CPU times are tabulated in Table 3. The zero-filling Fourier reconstruction in (a) shows that the data are really poor. The ℓ_1 -NN via e-BFGS method converges to a miserable solution. The residuals ($u_{\text{original}} - \hat{u}$) for all other methods are shown in Figure 9. It is quite surprising that ℓ_1 -TV (see Figures 8(d) and 9(b)) gives better visual and quantitative results (see Table 3) than the widely used ℓ_2 -TV (see Figures 8(c) and 9(a)). In Figure 8 (bottom row), the ℓ_2 -NN and our method seem to provide somewhat similar results. Nevertheless the residuals in Figures 9 and 10, as well as the quantitative assessment in Table 3, demonstrate that our method is much more precise than ℓ_2 -NN.

TABLE 3
PSNR and CPU time for all methods in Figures 8 relevant to 7% noisy data samples.

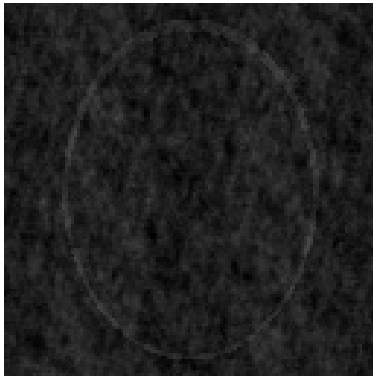
Method	ℓ_1 -NN via e-BFGS	ℓ_2 -TV	ℓ_1 -TV	ℓ_2 -NN	Our method
PSNR (dB)	14.23	27.47	30.58	45.48	75.64
CPU time (seconds)	2.88	8.11	2.61	33.48	48.94

Reconstructions from the 5% noisy data vector are naturally more sensitive, as seen in Figure 11. The corresponding PSNR values and CPU times are presented in Table 4. The ℓ_1 -NN via e-BFGS method in Figure 11(b) converges to an inane solution. The solutions produced by the *convex* methods ℓ_2 -TV and ℓ_1 -TV—see Figure 11(c)–(d)—recover up to some degree the outer shape of the phantom image, but its content is insignificant. The ℓ_2 -NN and our method (Figure 11, bottom row) recover quite correctly all shapes¹⁷ in the phantom image. However, the contrast in the ℓ_2 -NN reconstruction is underestimated, unlike that in the solution provided by our method.¹⁸ Indeed, the PSNR values in Table 4 confirm a nearly 44dB improvement

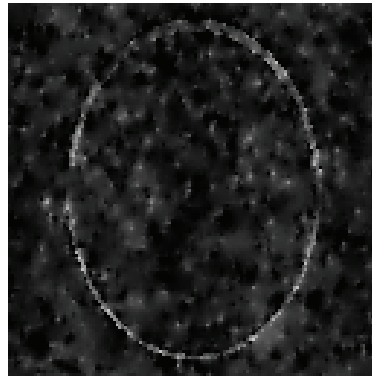
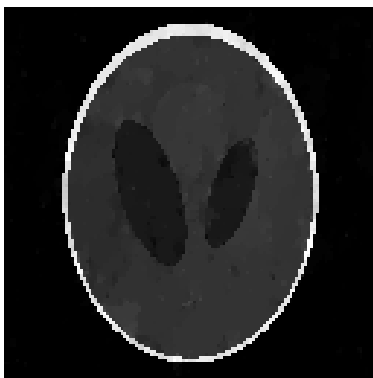
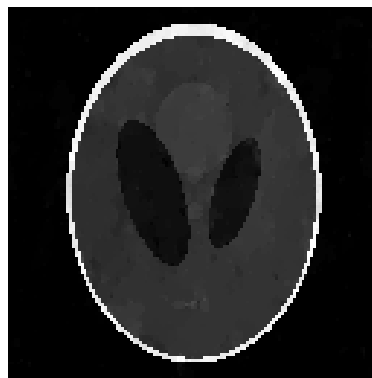
¹⁶Note that the method in [20] is in fact the very first step ($\varepsilon = 0$ and $k = 0$) in our numerical scheme in section 3.3.

¹⁷The success of ℓ_2 -NN can be explained by the dominant constant patches in the original image.

¹⁸We have already observed in Figure 5 that ℓ_1 -NN keeps a faithful contrast much better than ℓ_2 -NN does.



(a) Zero-filling Fourier recovery.

(b) ℓ_1 -NN via e-BFGS.(c) ℓ_2 -TV.(d) ℓ_1 -TV.(e) ℓ_2 -NN.

(f) Our method.

FIG. 8. Reconstructed images from 7% noisy randomly selected samples in the k -space using the different methods indicated.

for our method compared to ℓ_2 -NN. This quantitative evaluation is well corroborated by the error plots in Figure 12.

For both data vectors, our method outperforms its competitors both visually and quantitatively, as revealed by the figures and the PSNR values, respectively. Even

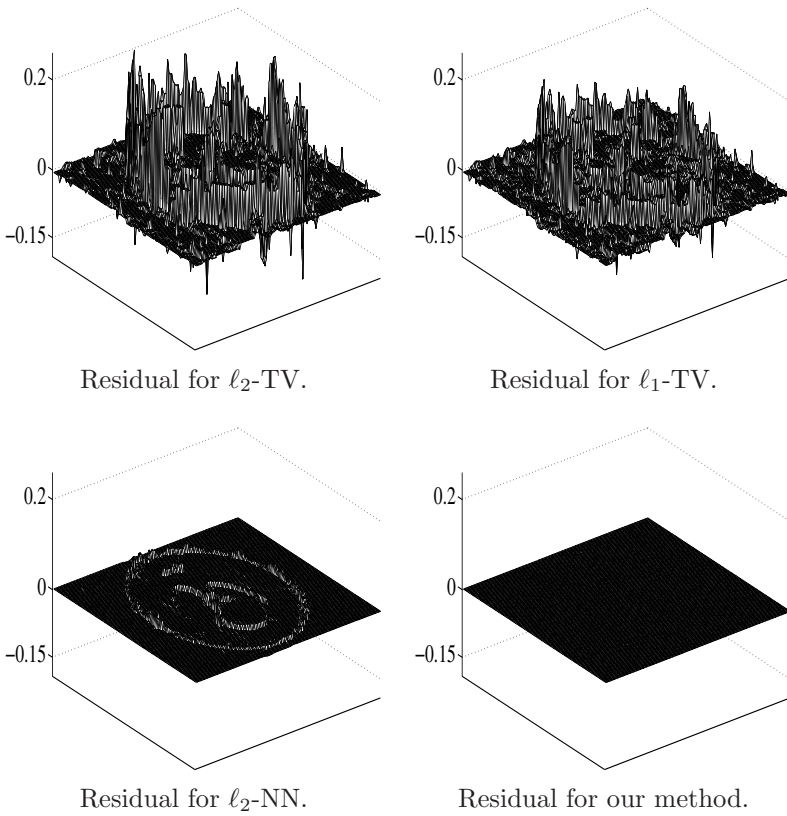


FIG. 9. Residuals (reconstructed image – recovered image) from 7% noisy randomly selected samples in the k -space for all successful methods in Figure 8. Recall that the gray-scale range of the original image is in $[0, 1]$.

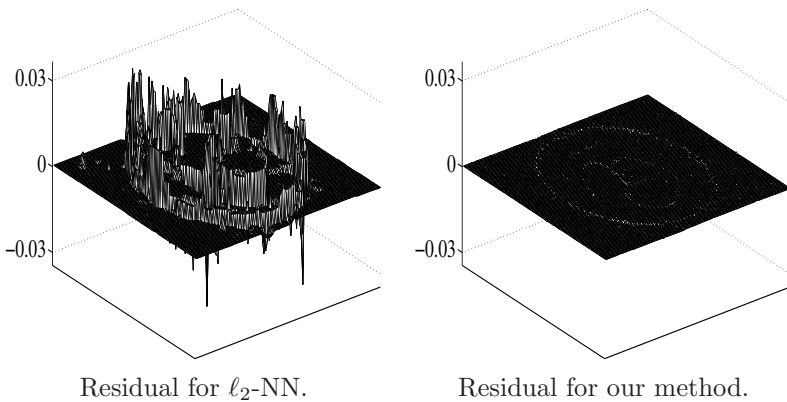
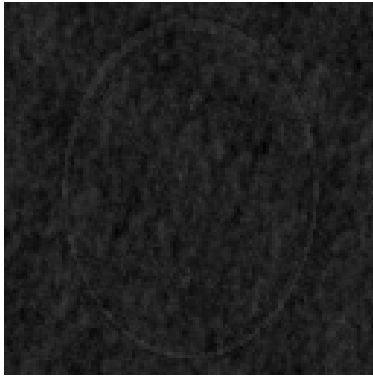
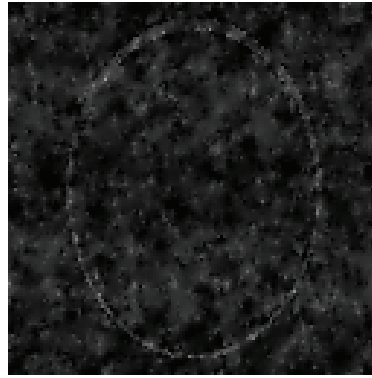
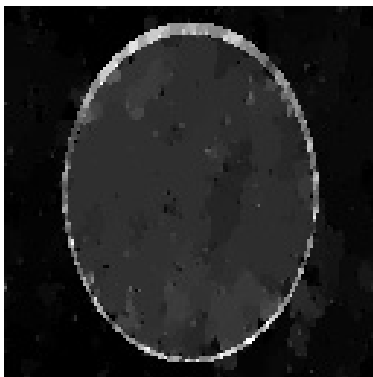
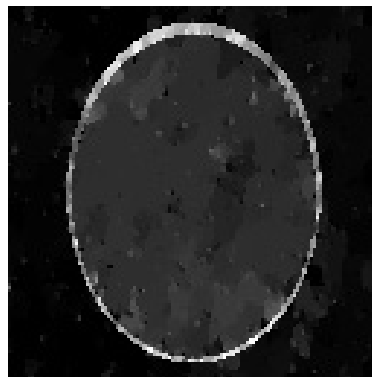


FIG. 10. Zoom along the z -axis of the residuals in Figure 9 for the ℓ_2 -NN and our method.

though it requires a higher computation load than the other methods, it remains comparatively reasonable. The pivotal improvement in the precision of MR image reconstructions enabled by our method justifies this increase in CPU time.



(a) Zero-filling Fourier recovery.

(b) ℓ_1 -NN via e-BFGS.(c) ℓ_2 -TV.(d) ℓ_1 -TV.(e) ℓ_2 -NN.

(f) Our method.

FIG. 11. Reconstructed images from 5% noisy randomly selected samples in the k -space using different methods.

4.3. Image deblurring under impulse noise. Data are generated as follows: the original image is blurred using a two-dimensional truncated Gaussian function,

$$(63) \quad h(s, t) = \exp\left(\frac{-s^2 - t^2}{2\sigma^2}\right) \quad \text{for } -3 \leq s, t \leq 3 \text{ and } \sigma = 1.5.$$

TABLE 4
PSNR and CPU time for all methods in Figure 11 corresponding to 5% noisy data samples.

Method	ℓ_1 -NN via e-BFGS	ℓ_2 -TV	ℓ_1 -TV	ℓ_2 -NN	Our method
PSNR (dB)	13.89	18.82	19.32	36.64	80.45
CPU time (seconds)	2.05	5.59	2.23	85.61	105.61

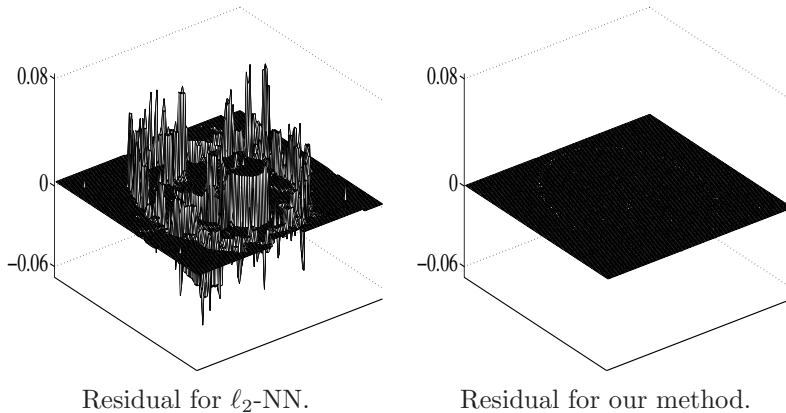


FIG. 12. Residuals (reconstructed image – recovered image) from 5% noisy randomly selected samples in the k -space for the ℓ_2 -NN and for our methods in Figure 11. Recall that the gray-scale range of the original image is in $[0, 1]$.

Data are produced by corrupting 30% of the pixels of the blurred image with salt-and-pepper (SP) impulse noise. The underlying image is the same as in Figure 7(a), and it is recalled for comparison reasons in Figure 7(f); the degraded image is shown in Figure 13(a).

The random degradation in the observed image affects only a part of the data samples. Hence the other part of data equations should be satisfied exactly. In a variational framework, the latter requires that the data fitting term be nonsmooth [32, 33]. So in this application we consider only ℓ_1 data fitting. The regularization term is defined as in the MRI example in subsection 4.2.

Our method is collated to the ℓ_1 -NN via e-BFGS and the ℓ_1 -TV methods as described in subsection 4.2. Deblurring of images corrupted with impulse noise using ℓ_1 -TV was recently explored in [46]. We also replaced all steps between “While relerr $> tol$ do” and “End While” in our algorithm (section 3.3), intended to solve (48) for any ε , by e-BFGS minimization [23]. The resultant *new* algorithm is called **ℓ_1 -NN via GNC & e-BFGS**.

Initialization of any e-BFGS-based numerical scheme with the observed image is now inappropriate as far as the condition that the cost function be differentiable at the starting point [23] is not satisfied.¹⁹ So we used a fully random initialization for both ℓ_1 -NN via e-BFGS and ℓ_1 -NN via GNC & e-BFGS numerical schemes. The other methods— ℓ_1 -TV and ours—were initialized with the observed image.

All restoration results are presented in Figure 13, while the relevant PSNR values and CPU times are seen in Table 5.

The ℓ_1 -NN via GNC & e-BFGS in (c) is better than the ℓ_1 -NN via e-BFGS

¹⁹Nevertheless, we tried both e-BFGS based schemes using the observed image, but the results were indeed pitiful.

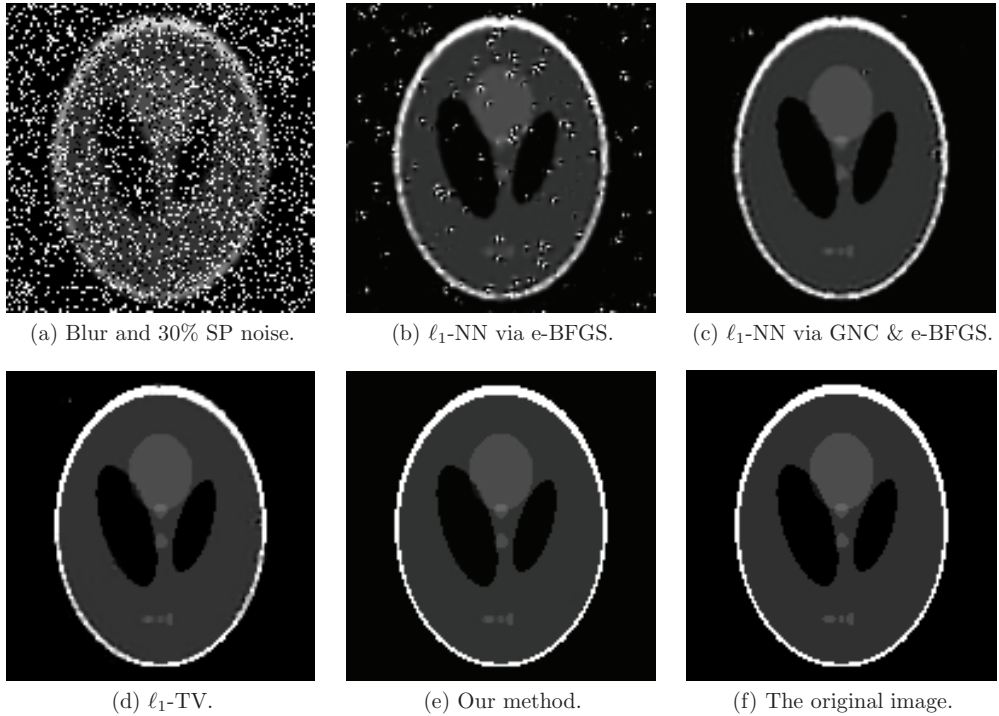


FIG. 13. The degraded image is shown in (a) and the underlying image in (f). Restorations of the latter image using different methods (b)–(e).

TABLE 5
PSNR and CPU time for all methods in Figure 13.

Method	ℓ_1 -NN via e-BFGS	ℓ_1 -NN via GNC & e-BFGS	ℓ_1 -TV	Our method
PSNR (dB)	15.58	23.37	29.22	44.89
CPU time (seconds)	5.82	314.41	12.48	141.11

scheme—see (b)—but visual results are worse than with the ℓ_1 -TV and our method, and ℓ_1 -NN via GNC & e-BFGS needs the highest CPU time among all restoration methods in Figure 13. The ℓ_1 -TV method in (d) recovers the main features of the underlying image well. However, a careful examination brings to light several artifacts near the interior boundary of the phantom and surrounding the right ellipsoid. Our method appears to be much more precise, as seen in Figure 13(e) and especially in the error plots in Figure 14.

We applied our method also using various initializations—e.g., a random or a flat image—and the obtained reconstruction results are almost the same. The method should be insensitive to initialization because the very first approximation solves a convex problem and the subsequent approximations are well-defined local minimizers.

In this applicative example, yet again, the method we propose (minimize \mathcal{F} in (6) using the algorithm in section 3.3) outperforms all competitors both visually and in terms of PSNR. The proposed method enables a much higher precision, especially in regions containing fine features.

5. Concluding remarks. In this paper, we proposed image reconstruction and image restoration using ℓ_1 data fitting combined with nonconvex nonsmooth regu-

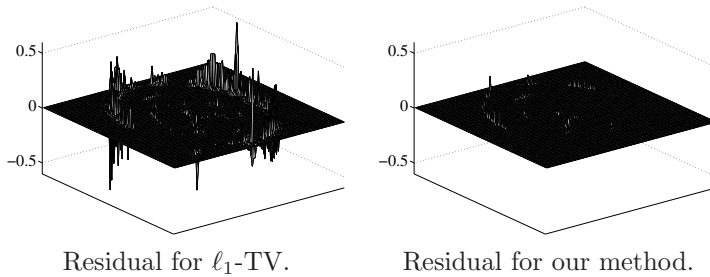


FIG. 14. Residuals (reconstructed image – recovered image) from 30% impulse noise. We recall that the original image is normalized on $[0, 1]$.

larization defined using strictly concave potential functions. Our theoretical results show that the solutions of the corresponding minimization problem are such that any pixel is involved in a data equation that is fitted exactly or in a null component of the regularization term. This remarkable property can be used in different ways in various imaging problems. From a practical side, we conceived a fast numerical scheme to solve this difficult minimization problem. Experimental results have shown the effectiveness of the proposed numerical scheme. To the best of our knowledge, this work is the first exploring this kind of cost function: the combination of ℓ_1 data fitting and nonconvex nonsmooth regularization. Naturally, many questions need a deeper exploration. These concern all aspects of the problem—theory, numerical issues, and other well-suited applications.

6. Appendix.

6.1. Proof of Proposition 1. It is important to notice that

$$(64) \quad \mathcal{F} \text{ in (6) is continuous and bounded below.}$$

With the aim of good pedagogy, we start with an easy particular case. Let one of the following conditions be verified:

- rank $A = p$;
- H1 holds and $\lim_{t \rightarrow +\infty} \varphi(t) = +\infty$;
- $\ker G = \{0\}$ and $\lim_{t \rightarrow +\infty} \varphi(t) = +\infty$.

In each one of these cases it is obvious that \mathcal{F} is coercive for any $v \in \mathbb{R}^q$. This, combined with (64), shows the result; see, e.g., [40].

Consider next the general case when rank A and rank G are arbitrary and φ can be bounded above. Let $u \in \mathbb{R}^p$ be arbitrarily fixed and $w \in \mathbb{R}^p \setminus \{0\}$ an arbitrary direction. According to H1, three cases arise for the direction w .

- (a) Let $w \in \ker G \setminus \{0\}$ if $\dim \ker G \geq 1$. By H1, $w \notin \ker A$. Then $Aw \neq 0$; hence

$$(65) \quad \mathcal{F}(u + w) = \|A(u + w) - v\|_1 \xrightarrow{\|w\| \rightarrow +\infty} +\infty.$$

- (b) Suppose that $w \in \ker A \setminus \{0\}$. Set

$$\nu \stackrel{\text{def}}{=} \max_{j \in J} \|G_j u\|_2.$$

By H1,

$$(66) \quad w \notin \ker G.$$

Then there exists a nonempty subset $\tilde{J} \subset J$ such that

$$\tilde{J} \stackrel{\text{def}}{=} \{j \in J \mid G_j w \neq 0\}.$$

Using (66) and the fact that $\ker A$ is a vector subspace, there exists $\mu_w > 0$ such that

$$\|w\|_2 > \mu_w \text{ and } j \in \tilde{J} \Rightarrow \|G_j w\|_2 \geq 2\nu + 1.$$

Then, using the definition of ν and the triangle inequality, we have

$$\begin{aligned} (67) \quad \|w\|_2 > \mu_w \text{ and } j \in \tilde{J} &\Rightarrow \|G_j w\|_2 \geq 2\|G_j u\|_2 + 1 \\ &\Rightarrow \|G_j w\|_2 > \|G_j u\|_2 \\ &\Rightarrow \|G_j(u + w)\|_2 \geq \|G_j w\|_2 - \|G_j u\|_2 > 0 \\ (68) &\Rightarrow \|G_j(u + w)\|_2 \geq \left| \|G_j w\|_2 - \|G_j u\|_2 \right|. \end{aligned}$$

Assumptions H2(a) and H2(b) show that φ is *strictly increasing* on \mathbb{R}_+ . Combining this property with (67) and (68) shows that

$$\begin{aligned} \|w\|_2 > \mu_w \text{ and } j \in \tilde{J} \Rightarrow \varphi(\|G_j(u + w)\|_2) &\geq \varphi\left(\left| \|G_j w\|_2 - \|G_j u\|_2 \right|\right) \\ &\geq \varphi\left(\left| 2\|G_j u\|_2 + 1 - \|G_j u\|_2 \right|\right) \\ &= \varphi(\|G_j u\|_2 + 1) \\ &> \varphi(\|G_j u\|_2). \end{aligned}$$

Inserting the latter result into the expression of \mathcal{F} shows that

$$\begin{aligned} \|w\|_2 > \mu_w \Rightarrow \mathcal{F}(u + w) &= \|A(u + w) - v\|_1 + \beta \sum_{j \in J} \varphi(\|G_j(u + w)\|_2) \\ &= \|Au - v\|_1 + \beta \sum_{j \in J} \varphi(\|G_j(u + w)\|_2) \\ (69) \quad &> \|Au - v\|_1 + \beta \sum_{j \in J} \varphi(\|G_j u\|_2) = \mathcal{F}(u). \end{aligned}$$

(c) Last, consider that $w \in \mathbb{R}^p \setminus \{\ker A \cup \ker G\}$, $w \neq 0$. Then $Aw \neq 0$, so

$$(70) \quad \mathcal{F}(u + w) = \|A(u + w) - v\|_1 + \beta \sum_{j \in J} \varphi(\|G_j(u + w)\|_2) \xrightarrow{\|w\| \rightarrow +\infty} +\infty.$$

The results obtained in (65), (69), and (70) show that \mathcal{F} is asymptotically strictly increasing in any direction $w \in \mathbb{R}^p$. Consequently,

$$\inf_{u' \in \mathbb{R}^p} \mathcal{F}(u') \leq \mathcal{F}(u) < \mathcal{F}(u + w) \text{ as } \|w\|_2 \rightarrow +\infty \quad \forall w \in \mathbb{R}^p.$$

This fact, combined with (64), shows that for all $v \in \mathbb{R}^q$ the optimal set \hat{U} is nonempty.

6.2. Proof of Lemma 1. Saying that $u \in B(\hat{u}, \rho)$ is equivalent to $u = \hat{u} + w$ for $\|w\|_2 < \rho$. Consider an arbitrary $w \in B(0, \rho)$.

Let $\widehat{I}_0^c \neq \emptyset$. Since $\rho \leq \min_{i \in \widehat{I}_0^c} \frac{|a_i \hat{u} - v[i]|}{\|a_i\|_2}$, we have $\|w\|_2 < \min_{i \in \widehat{I}_0^c} \frac{|a_i \hat{u} - v[i]|}{\|a_i\|_2}$. Then

$$\begin{aligned} i \in \widehat{I}_0^c &\Rightarrow \psi_i(\hat{u} + w) = |a_i(\hat{u} + w) - v[i]| \geq |a_i \hat{u} - v[i]| - |a_i w| \\ &\geq |a_i \hat{u} - v[i]| - \|a_i\|_2 \|w\|_2 \\ &= \|a_i\|_2 \left(\frac{|a_i \hat{u} - v[i]|}{\|a_i\|_2} - \|w\|_2 \right) \\ &\geq \|a_i\|_2 \left(\min_{i \in \widehat{I}_0^c} \frac{|a_i \hat{u} - v[i]|}{\|a_i\|_2} - \|w\|_2 \right) > 0. \end{aligned}$$

Hence (17).

Consider that $\widehat{J}_0^c \neq \emptyset$. Since $\rho \leq \min_{j \in \widehat{J}_0^c} \frac{\|G_j \hat{u}\|_2}{\|G_j\|_2}$, then $\|w\|_2 < \min_{j \in \widehat{J}_0^c} \frac{\|G_j \hat{u}\|_2}{\|G_j\|_2}$. In a similar way as above,

$$\begin{aligned} j \in \widehat{J}_0^c &\Rightarrow \|G_j(\hat{u} + w)\|_2 \geq \|G_j \hat{u}\|_2 - \|G_j w\|_2 \geq \|G_j \hat{u}\|_2 - \|G_j\|_2 \|w\|_2 \\ &= \|G_j\|_2 \left(\frac{\|G_j \hat{u}\|_2}{\|G_j\|_2} - \|w\|_2 \right) \\ &\geq \|G_j\|_2 \left(\min_{j \in \widehat{J}_0^c} \frac{\|G_j \hat{u}\|_2}{\|G_j\|_2} - \|w\|_2 \right) > 0. \end{aligned}$$

Combining this result with the fact that φ in (16) is \mathcal{C}^2 on \mathbb{R}_+^* , by H2(a), leads to (18).

REFERENCES

- [1] H. ATTOUCH, J. BOLTE, AND F. SVAITER, *Convergence of descent methods for semi-algebraic and tame problems: Proximal algorithms, forward-backward splitting, and regularized Gauss–Seidel methods*, Math. Program., (2011).
- [2] G. AUBERT AND P. KORNPROBST, *Mathematical Problems in Image Processing*, 2nd ed., Springer-Verlag, Berlin, 2006.
- [3] J.-F. AUJOL, G. GILBOA, T. CHAN, AND S. OSHER, *Structure-texture image decomposition—Modeling, algorithms, and parameter selection*, Int. J. Comput. Vision, 67 (2006), pp. 111–136.
- [4] L. BAR, A. BROOK, N. SOCHEN, AND N. KIRYATI, *Deblurring of color images corrupted by salt-and-pepper noise*, IEEE Trans. Image Process., 16 (2007), pp. 1101–1111.
- [5] M. BELGE, M. KILMER, AND E. MILLER, *Wavelet domain image restoration with adaptive edge-preserving regularization*, IEEE Trans. Image Process., 9 (2000), pp. 597–608.
- [6] J. E. BESAG, *Digital image processing: Towards Bayesian image analysis*, J. Appl. Statist., 16 (1989), pp. 395–407.
- [7] A. BLAKE AND A. ZISSERMAN, *Visual Reconstruction*, MIT Press, Cambridge, MA, 1987.
- [8] M. BLACK AND A. RANGARAJAN, *On the unification of line processes, outlier rejection, and robust statistics with applications to early vision*, Int. J. Comput. Vision, 19 (1996), pp. 57–91.
- [9] A. M. BRUCKSTEIN, D. L. DONOHO, AND M. ELAD, *From sparse solutions of systems of equations to sparse modeling of signals and images*, SIAM Rev., 51 (2009), pp. 34–81.
- [10] T. F. CHAN AND S. ESEDOĞLU, *Aspects of total variation regularized L^1 function approximation*, SIAM J. Appl. Math., 65 (2005), pp. 1817–1837.
- [11] T. F. CHAN, S. ESEDOĞLU, AND M. NIKOLOVA, *Algorithms for finding global minimizers of image segmentation and denoising models*, SIAM J. Appl. Math., 66 (2006), pp. 1632–1648.
- [12] S. DURAND AND M. NIKOLOVA, *Denoising of frame coefficients using l^1 data-fidelity term and edge-preserving regularization*, Multiscale Model. Simul., 6 (2007), pp. 547–576.
- [13] S. DURAND, J. FADILI, AND M. NIKOLOVA, *Multiplicative noise removal using l_1 fidelity on frame coefficients*, J. Math. Imaging Vision, 19 (2010), pp. 201–226.

- [14] V. DUVAL, J.-F. AUJOL, AND Y. GOUSSEAU, *The TVL1 model: A geometric point of view*, Multiscale Model. Simul., 8 (2009), pp. 154–189.
- [15] H. FU, M. K. NG, M. NIKOLOVA, AND J. L. BARLOW, *Efficient minimization methods of mixed ℓ_2 - ℓ_1 and ℓ_1 - ℓ_1 norms for image restoration*, SIAM J. Sci. Comput., 27 (2006), pp. 1881–1902.
- [16] D. GEMAN AND G. REYNOLDS, *Constrained restoration and recovery of discontinuities*, IEEE Trans. Pattern Anal. Machine Intell., 14 (1992), pp. 367–383.
- [17] D. GEMAN AND C. YANG, *Nonlinear image recovery with half-quadratic regularization*, IEEE Trans. Image Process., 4 (1995), pp. 932–946.
- [18] S. GEMAN AND D. GEMAN, *Stochastic relaxation, Gibbs distributions, and the Bayesian restoration of images*, IEEE Trans. Pattern Anal. Machine Intell., 6 (1984), pp. 721–741.
- [19] R. GONZALEZ AND R. WOODS, *Digital Image Processing*, 3rd ed., Pearson, London, 2008.
- [20] X. GUO, F. LI, AND M. K. NG, *A fast ℓ_1 -TV algorithm for image restoration*, SIAM J. Sci. Comput., 31 (2009), pp. 2322–2341.
- [21] M. HOFER, T. POCK, K. KAPP, T. BAUERNHOFER, F. EBNER, AND R. STOLLBERGER, *DCE-MRI tumor registration by using TV- L^1 optical flow*, in Proceedings of the 17th Scientific Meeting of the International Society for Magnetic Resonance in Medicine, 2009, pp. 46–59.
- [22] A. JAIN, *Fundamentals of Digital Image Processing*, Prentice-Hall, Englewood Cliffs, NJ, 1989.
- [23] A. S. LEWIS AND M. L. OVERTON, *Nonsmooth optimization via quasi-Newton methods*, Math. Program., Online First, February, 2012, <http://link.springer.com/article/10.1007/s10107-012-0514-2>.
- [24] Q. LIN, *Sparsity and Nonconvex Nonsmooth Optimization*, Proquest Dissertation Publishing, Ann Arbor, MI, 2011.
- [25] Y. LIU AND Y. WU, *Variable selection via a combination of the ℓ_0 and ℓ_1 penalties*, J. Comput. Graphical Statist., 16 (2007), pp. 782–798.
- [26] M. LUSTIG, D. DONOHO, AND J. M. PAULY, *Sparse MRI: The application of compressed sensing for rapid MR imaging*, Magn. Reson. Med., 58 (2007), pp. 1182–1195.
- [27] M. LUSTIG, D. DONOHO, J. M. SANTOS, AND L. M. PAULY, *Compressed Sensing MRI: A look how CS can improve our current imaging techniques*, IEEE Signal Process. Mag., 25 (2008), pp. 72–82.
- [28] J. LV AND Y. FAN, *A unified approach to model selection and sparse recovery using regularized least squares*, Ann. Statist., 37 (2009), pp. 3498–3528.
- [29] M. NG AND N. BOSE, *Mathematical analysis of super-resolution methodology*, IEEE Signal Process. Mag., 20 (2003), pp. 62–74.
- [30] M. K. NG, R. H. CHAN, AND W. C. TANG, *A fast algorithm for deblurring models with Neumann boundary conditions*, SIAM J. Sci. Comput., 21 (1999), pp. 851–866.
- [31] M. NIKOLOVA, *Markovian reconstruction using a GNC approach*, IEEE Trans. Image Process., 8 (1999), pp. 1204–1220.
- [32] M. NIKOLOVA, *Minimizers of cost-functions involving nonsmooth data-fidelity terms. Application to the processing of outliers*, SIAM J. Numer. Anal., 40 (2002), pp. 965–994.
- [33] M. NIKOLOVA, *A variational approach to remove outliers and impulse noise*, J. Math. Imaging Vision, 20 (2004), pp. 99–120.
- [34] M. NIKOLOVA, *Analysis of the recovery of edges in images and signals by minimizing nonconvex regularized least-squares*, Multiscale Model. Simul., 4 (2005), pp. 960–991.
- [35] M. NIKOLOVA, M. K. NG, S. ZHANG, AND W. K. CHING, *Efficient reconstruction of piecewise constant images using nonsmooth nonconvex minimization*, SIAM J. Imaging Sci., 1 (2008), pp. 2–25.
- [36] M. NIKOLOVA, M. NG, AND C. TAM, *Fast nonconvex nonsmooth minimization methods for image restoration and reconstruction*, IEEE Trans. Image Process., 19 (2010), pp. 3073–3088.
- [37] J. NOCEDAL AND S. WRIGHT, *Numerical Optimization*, Springer, New York, 1999.
- [38] T. POCK, M. URSCHLER, C. ZACH, R. BEICHEL, AND H. BISHOF, *A duality based algorithm for TV- L^1 -optical-flow image registration*, in Proceedings of the 10th international Conference on Medical Image Computing and Computer Assisted Intervention (MICCAI), Lecture Notes in Comput. Sci. 4792, Springer, New York, 2007, pp. 511–518.
- [39] L. L. RAKÉT, L. ROHLM, M. NIELSEN, AND F. LAUZE, *TV- L^1 optical flow for vector valued images*, in Proceedings of the Conference on Energy Minimization Methods in Computer Vision and Pattern Recognition, Lecture Notes in Comput. Sci. 6819, Springer, 2011, pp. 329–343.
- [40] R. T. ROCKAFELLAR AND J. B. WETS, *Variational Analysis*, Springer-Verlag, Berlin, 1997.
- [41] L. RUDIN, S. OSHER, AND C. FATEMI, *Nonlinear total variation based noise removal algorithm*, Phys. D, 60 (1992), pp. 259–268.

- [42] D. STRONG AND T. F. CHAN, *Edge-preserving and scale-dependent properties of total variation regularization*, *Inverse Problems*, 19 (2003), pp. S165–S187.
- [43] Y. WANG, J. YANG, W. YIN, AND Y. ZHANG, *A new alternating minimization algorithm for total variation image reconstruction*, *SIAM J. Imaging Sci.*, 1 (2008), pp. 248–272.
- [44] E. WASSERSTROM, *Numerical solutions by the continuation method*, *SIAM Rev.*, 15 (1973), pp. 89–119.
- [45] A. WEDEL, T. POCK, C. ZACH, H. BISCHOF, AND D. CREMERS, *An improved algorithm for TV- L^1 optical flow*, in *Statistical and Geometrical Approaches to Visual Motion Analysis*, Springer-Verlag, Berlin, Heidelberg, 2009, p. 23–45.
- [46] J. YANG, Y. ZHANG, AND W. YIN, *An efficient TVL1 algorithm for deblurring multichannel images corrupted by impulsive noise*, *SIAM J. Sci. Comput.*, 31 (2009), pp. 2842–2865.
- [47] J. YANG, W. YIN, Y. ZHANG, AND Y. WANG, *A fast algorithm for edge-preserving variational multichannel image restoration*, *SIAM J. Imaging Sci.*, 2 (2009), pp. 569–592.
- [48] C. ZACH, T. POCK, AND H. BISCHOF, *A duality based approach for realtime TV- L^1 optical flow*, in *Pattern Recognition (Proc. DAGM)*, Heidelberg, Germany, 2007, pp. 214–223.